Trends in Inversion Barriers of Group 15 Compounds. 2. *Ab-Initio* and Density Functional Calculations on Group 15 Fluorides

Peter Schwerdtfeger,* Peter D. W. Boyd, Thomas Fischer,† Patricia Hunt, and Michael Liddell

Contribution from the Computational Materials Science and Engineering Unit (CMSE), Department of Chemistry, University of Auckland, Private Bag 92019, Auckland, New Zealand

Received March 29, 1994⊗

Abstract: Two-dimensional hypersurfaces for the inversion process of the group 15 fluorides MF_3 (M = N, P, As, Sb, Bi) involving the MF_3 umbrella motion and the symmetric F–M–F bending mode have been calculated at the Hartree–Fock level. The MO scheme of NF_3 shows an a_2'' HOMO and a_1' LUMO in accordance with the frontier orbitals of the group 15 hydrides, and therefore it inverts through the expected trigonal planar D_{3h} transition state. For PF_3, AsF_3, SbF_3, and BiF_3, however, the HOMO–LUMO sequence is inverted and the HOMO is of a_1' symmetry. This results in an $a_1'_{HOMO} \otimes e'_{LUMO}$ mixing at the trigonal planar D_{3h} structure causing a second-order Jahn–Teller symmetry breaking (distortion Hamiltonian is of e' symmetry) toward the T-shaped C_{2v} arrangement. The minimum energy inversion path is of C_s symmetry starting from the pyramidal C_{3v} minimum structure by distorting immediately toward the T-shaped C_{2v} first-order transition state. Møller–Plesset second-order results (MP2) are compared with local density functional approximation (LDA) methods including nonlocal corrections and several semiempirical (AM1, PM3, and MNDO) calculations. The performance of different exchange and correlation functionals within LDA including gradient corrections is discussed in detail. Because of the $a_1'_{HOMO} \otimes e'_{LUMO}$ mixing, electron correlation contributions become very important and Freed's theorem is not valid for the fluorides of the heavier elements P, As, Sb, and Bi. Hence, to assess the validity of a single-determinant MP2 approach we performed complete active space MP2 calculations (CASPT2) for the minimum and inversion structures of NF_3 and PF_3. These calculations show that for PF_3 a multireference scheme is necessary to describe the energetics of the D_{3h} to C_{2v} Jahn–Teller distortion accurately. The inversion barrier from the C_{3v} minimum structure to the C_{2v} inversion point is, however, satisfactorily described by a single-reference MP2 procedure. Vibrational frequencies and structure are predicted for gas-phase BiF_3 at the MP2 level. The relativistic change in the F–Bi–F bond angle is large ($\alpha^{NR} - \alpha^{R} = -1.5°$ at the MP2 level), resulting in an anomaly in the trend of F–M–F bond angles along the group 15 fluorides. When the vibrational frequencies are considered, MP2 of all the methods performs the best while, somewhat surprisingly, the Becke correction to the LDA exchange functional leads to large errors. Despite this, the LDA inversion barriers seem to be more accurate than the single-reference MP2 values, and in the case of PF_3 both the LDA (using the Vosko–Wilk–Nusair (VWN) parametrization) and the CASPT2 method are in close agreement. For BiF_3 at the relativistic level, LDA/VWN and PM3 predict a trigonal planar inversion structure contradicting MP2 and coupled cluster results. However, if relativistic effects are neglected, both LDA and MP2 yield a T-shaped inversion state.

I. Introduction

Pyramidal inversion of MX_3 molecules usually involves a transition through an inversion point of D_{3h} symmetry.[1-7] This may not be generalized to MX_n molecules where $n > 3$, as has been demonstrated recently by Gordon and Schmidt for the molecule CH_4.[8] It came, however, as a surprise when Dixon and Arduengo[9-13] showed that some of the group 15 fluorides prefer a T-shaped planar transition structure. This has been verified experimentally for ADPO compounds using NMR techniques.[6,10] Marynick pointed out that in the trigonal planar D_{3h} arrangement of PF_3 and AsF_3 the expected HOMO–LUMO sequence is interchanged ($a_1' \leftrightarrow a_2''$).[14-16] Recently, Edgecombe used Bader's topological analysis of the electron density to discuss the two different transition-state structures of PH_3 and PF_3.[17] Nevertheless, a definitive explanation for the symmetry breaking from D_{3h} into C_{2v} symmetry has not yet been put forward. As a result of this distortion, the inversion process cannot be simplified any more by a one-dimensional double-minimum potential curve, which, in the past, has been useful for the calculation of tunneling splittings of MH_3 inversion modes.[7] To approximately describe the inversion through a C_{2v} transition state one has to consider at least two (possibly three) internal coordinates, the usual C_3–M–X inversion angle (a_1 mode; C_3 denotes the C_3-axis of the MX_3 molecule in the local C_{3v} symmetry) and the symmetric X–M–X bending angle (doubly degenerate e mode). This

† Alexander von Humboldt Feodor Lynen fellow.

(1) Weston, R. E. *J. Am. Chem. Soc.* **1954**, *76*, 2645.
(2) Swalen, J. D.; Ibers, J. A. *J. Chem. Phys.* **1962**, *36*, 1914.
(3) (a) Allen, L. C.; Rauk, A.; Mislow, K. *Angew. Chem., Int. Ed. Engl.* **1970**, *9*, 400. (b) Lambert, J. B. In *Topics in Stereochemistry*; Allinger, N. L., Eliel, E. L., Eds.; Wiley: New York, 1971; Vol. 6.
(4) Baechler, R. D.; Andose, J. D.; Stackhouse, J.; Mislow, K. *J. Am. Chem. Soc.* **1972**, *94*, 8060.
(5) Levin, C. C. *J. Am. Chem. Soc.* **1975**, *97*, 5649.
(6) Arduengo, A. J.; Dixon, D. A. In *Heteroatom Chemistry*; Block, E., Ed.; VCH Publ.: New York, 1990.
(7) Schwerdtfeger, P.; Laakkonen, L.; Pyykkö, P. *J. Chem. Phys.* **1992**, *96*, 6807.
(8) Gordon, M. S.; Schmidt, M. W. *J. Am. Chem. Soc.* **1993**, *115*, 7486.
(9) Dixon, D. A.; Arduengo, A. J.; Fukunaga, T. *J. Am. Chem. Soc.* **1986**, *108*, 2461.
(10) Arduengo, A. J.; Dixon, D. A.; Roe, D. C. *J. Am. Chem. Soc.* **1986**, *108*, 6821.
(11) Dixon, D. A.; Arduengo, A. J. *J. Am. Chem. Soc.* **1987**, *109*, 338.
(12) Dixon, D. A.; Arduengo, A. J. *J. Chem. Soc., Chem. Commun.* **1987**, 498.
(13) Dixon, D. A.; Arduengo, A. J. *Int. J. Quantum Chem., Quantum Chem. Symp.* **1988**, No. 22, 85.
(14) Marynick, D. S. *Chem. Phys. Lett.* **1980**, *71*, 101.
(15) Marynick, D. S. *J. Chem. Phys.* **1980**, *73*, 3939.
(16) Marynick, D. S.; Rosen, D. C.; Liebman, J. F. *J. Mol. Struct. (THEOCHEM)* **1983**, *94*, 47.
(17) Edgecombe, K. E. *J. Mol. Struct. (THEOCHEM)* **1991**, *226*, 157.

0002-7863/94/1516-9620$04.50/0

definition of a two-dimensional potential hypersurface may give insight into the mechanism of this unusual symmetry breaking, i.e., the deviation from the C_{3v} minimum energy inversion path (MEIP).

Deviations from an expected molecular geometry can often be rationalized with the use of the Jahn–Teller (JT) theorem.[18,19] Whereas the first-order JT contribution must lead to a distortion for certain molecular symmetries and electronic configurations, second and higher order terms may or may not result in a symmetry breaking of the molecular geometry. For example, compare the isoelectronic molecules CH_3 (minimum D_{3h} symmetry) and SiH_3 (minimum C_{3v} symmetry).[20] Within the Born–Oppenheimer approximation the second-order (static) JT term is proportional to the infinite sum over electronic excited state contributions,[21,22] $[\langle 0|H_q|n\rangle^2(E_0-E_n)^{-1}]$. H_q is the first derivative of the electronic Hamiltonian with respect to the distortion coordinate q, $|n\rangle$ is the electronic excited state wave function (in the usual Dirac notation), and E_0 and E_n denote the ground and excited electronic states, respectively. An important term in this equation is the size of the energy difference $(E_0 - E_n)$, which can be estimated from orbital energy differences (HOMO–LUMO energy gap). If there is a low-lying excited state $|n\rangle$ with $\langle 0|H_q|n\rangle \neq 0$, and if the difference (E_0-E_n) is sufficiently small, then the second derivative of the total electronic energy E with respect to the distortion coordinate q can become negative and distortion occurs in either direction, $q < q_0$ and $q > q_0$ (q_0 denotes the point along the distortion coordinate q before symmetry breaking occurs). This is the basic idea behind the use of frontier orbital theory in the discussion of second-order JT distortions. For example, ClF_3 is well-known to adopt a planar T-shaped minimum structure, which has been explained by a second-order JT distortion.[23] We will attempt to apply this principle to the symmetry breaking of group 15 fluorides starting from the planar MF_3 arrangement.

The inversion barriers within the group 15 hydrides increase monotonically from NH_3 to BiH_3.[3] Mislow *et al.* pointed out that a sound theoretical basis explaining this trend is still missing.[3] However, the increase in the barrier heights down the group 15 hydrides can be rationalized using frontier orbital theory in connection with a second-order JT distortion.[7] In contrast, the barrier heights for fluorides decrease along the series from NF_3 to BiF_3.[7,11] The reason for this behavior is not understood, and it contradicts earlier assumptions that the increasing barrier height is related to a decreasing X–M–X angle.[3,7] Moreover, NF_3 seems to have an unusually high inversion barrier, suggesting that some nitrogen-containing compounds of the form $NL_1L_2L_3$ with different ligands L_1, L_2, and L_3 may be optically active on an experimentally reasonable time scale.[24] It is therefore of interest to study the trend in inversion barriers of compounds containing group 15 elements.

Inversion barriers are sensitive to electronic effects such as inductive, delocalization, and hyperconjugative effects.[3] It is generally accepted that electropositive ligands X lead to low inversion barriers while electronegative ligands increase the barrier height.[25,26] For example, a comparison between inversion barriers of second- and third-row main group hydrides and fluorides MX_3 (X = H, F) supports this assumption.[27] We will analyze this in some detail, and it will seen if this assumption can be generalized to all group 15 element containing compounds.

In the last decade density functional theory has become a powerful tool for molecular calculations involving a large number of atoms. Standard program packages are now available, and several review articles and books have been dedicated to this method.[28] Besides some serious drawbacks of current density functional theory (such as the treatment of weak interactions between atoms and molecules, and the problem of electronically excited states), it is now a generally accepted and widely used method in quantum chemistry of molecules and the solid state. It is well-known that current local density approximations (LDA) can incorporate relatively large errors in the calculation of energy differences, which is due to the error incorporated in the exchange-correlation functional.[29] To address this problem, several gradient corrections for both the exchange and correlation functionals have been proposed.[28] However, very recently Yang *et al.* pointed out that LDA including gradient corrections fails to predict the correct trend of exchange and correlation energies as the atomic charge increases.[30] Most of the computational work reported to date seems to be focused on comparison of ionization potentials of atoms, atomization energies, and the structure of smaller molecules to establish the quality of the functional in use.[28-32] Less intensive studies have been done on other molecular[33] properties such as the force field (vibrational harmonic spectrum), inversion barriers, etc. If a symmetry-broken inversion point can be explained in terms of frontier orbital theory, then we expect that all reliable quantum chemical approximations should be able to account for such effects. The comparison between LDA and the well-established MP2 method for the calculation of inversion barriers was therefore of particular interest in the present study.

In this second work on inversion processes[7] we present *ab initio* Hartree–Fock (HF), Møller–Plesset second-order (MP2), and local density functional (LDA) including gradient corrections as well as semiempirical calculations (AM1, PM3, and MNDO) for all group 15 fluorides MF_3 (M = N, P, As, Sb, and Bi). To date very little theoretical work has been carried out on the late group 15 halides. NF_3,[11,15,26,27,34-41] PF_3,[9,11,12,15-17,26,27,36-43] and AsF_3[11,16,27,41,44-47] have been studied in some more detail, but

(18) (a) Jahn, H. A.; Teller, E. *Proc. R. Soc. London, A* **1937**, *161*, 220. (b) Jotham, R. W.; Kettle, S. F. A. *Inorg. Chim. Acta* **1971**, *5*, 180.
(19) Liehr, A. D. *J. Chem. Phys.* **1957**, *27*, 476.
(20) (a) Liebmann, J. F. *J. Am. Chem. Soc.* **1974**, *96*, 3053. (b) Liebmann, J. F.; Vincent, J. C. *J. Am. Chem. Soc.* **1975**, *97*, 1373. (c) Jachel, G. S.; Gordy, W. *Phys. Rev.* **1968**, *176*, 443.
(21) (a) Liehr, A. D. *J. Phys. Chem.* **1963**, *67*, 389. (b) Pearson, R. *J. Am. Chem. Soc.* **1969**, *91*, 1252. (c) Pearson, R. *J. Am. Chem. Soc.* **1969**, *91*, 4947. (d) Pearson, R. *J. Chem. Phys.* **1970**, *52*, 2167. (e) Öpik, V.; Pryce, M. H. L. *Proc. R. Soc. London* **1957**, *A238*, 425. (f) Bader, R. F. W. *Can. J. Chem.* **1962**, *40*, 1164.
(22) Burdett, J. K. *Chem. Soc. Rev.* **1978**, 507.
(23) Bartell, L. S. *J. Chem. Educ.* **1968**, *45*, 754.
(24) The highest barrier for a nitrogen-containing compound was estimated for $NOCPh_2CH_3$ with a barrier of 145 kJ/mol; see: Montanari, F.; Moretti, I.; Torre, G. *J. Chem. Soc., Chem. Commun.* **1969**, 1086.
(25) Liebman, J. F.; Politzer, P.; Sanders, W. A. *J. Am. Chem. Soc.* **1976**, *98*, 5115.
(26) Boldyrev, A. I.; Charkin, O. P. *J. Struct. Chem.* **1985**, *26*, 451; *Zh. Struct. Chim.* **1985**, *26*, 158.
(27) Clotet, A.; Rubio, J.; Illas, F. *J. Mol. Struct. (THEOCHEM)* **1988**, *164*, 351.
(28) (a) Barth, U. v. In *Many-Body Phenomena at Surfaces*; Langreth, D. C., Suhl, H., Eds.; Academic: New York, 1984. (b) Jones, R. O.; Gunnarsson, O. *Rev. Mod. Phys.* **1989**, *61*, 689. (c) Parr, R. G.; Yang, W. *Density-Functional Theory of Many-Electron Systems*; Oxford University Press: New York, 1989. (d) Kryachko, E. S.; Ludena, E. V. *Density-Functional Theory of Many-Electron Systems*; Kluwer: Dordrecht, 1991. (e) March, M. H. *Electron Density Theory of Atoms and Molecules*; Academic: New York, 1992. (f) Ziegler, T. *Chem. Rev.* **1991**, *91*, 651.
(29) Becke, A. D. *J. Chem. Phys.* **1993**, *98*, 5648.
(30) Zhu, T.; Lee, C.; Yang, W. *J. Chem. Phys.* **1993**, *98*, 4814.
(31) Becke, A. D. *J. Chem. Phys.* **1992**, *96*, 2155.
(32) Laming, G. J.; Termath, V.; Handy, N. C. *J. Chem. Phys.* **1993**, *99*, 8765.
(33) Johnson, B. G.; Gill, P. M. W.; Pople, J. A. *J. Chem. Phys.* **1993**, *98*, 5612.
(34) Mack, H. G.; Christen, D.; Oberhammer, H. *J. Mol. Struct.* **1988**, *190*, 215.
(35) Dixon, D. A. *J. Chem. Phys.* **1985**, *109*, 83.
(36) Versluis, L.; Ziegler, T. *J. Chem. Phys.* **1988**, *88*, 322.
(37) Delley, B. *J. Chem. Phys.* **1991**, *94*, 7245.
(38) Xiao, S. X.; Trogler, W. C.; Ellis, D. E.; Berkovitch-Yellin, Z. *J. Am. Chem. Soc.* **1983**, *105*, 7033.
(39) Schmiedekamp, A.; Skaarup, S.; Pulay, P.; Boggs, J. E. *J. Chem. Phys.* **1977**, *66*, 5769.
(40) (a) Reed, A. E.; Schleyer, P. v. R. *J. Am. Chem. Soc.* **1987**, *109*, 7362. (b) Reed, A. E.; Schleyer, P. v. R. *J. Am. Chem. Soc.* **1990**, *112*, 1434.
(41) Breidung, J.; Thiel, W. *J. Comput. Chem.* **1992**, *13*, 165.
(42) Breidung, J.; Thiel, W. *J. Phys. Chem.* **1988**, *92*, 165.
(43) Fowler, P. W.; Kelly, H. M.; Sadlej, A. J. *Chem. Phys. Lett.* **1993**, *212*, 659.
(44) Breidung, J.; Thiel, W.; Komornicki, A. *Inorg. Chem.* **1991**, *30*, 1067.

there are only a few investigations of SbF_3[11,41,47,48] and BiF_3.[41,49] There is also scant experimental data for BiF_3. Thus, we predict molecular properties at the MP2, LDA, and PM3 levels. We present two-dimensional Hartree–Fock inversion hypersurfaces in order to evaluate the minimum energy inversion path and the mechanism of the symmetry breaking from the expected C_{3v} arrangement to the C_s structure. The methods used are described in detail in the next section. Results and discussion are presented in section III. A summary is given in section IV.

II. Computational Methods

Hartree–Fock (HF) calculations for the group 15 fluorides MF_3 ($^1A_1$; C_{3v}), MF_2 ($^2B_1$; C_{2v}), and MF ($^3\Sigma^-$ only) were performed using GAUSSIAN92/DFT.[50] Relatively large basis sets were used for N, P, As, Sb, Bi, and F. The basis sets for the group 15 atoms are described in detail in ref 7. For fluorine a 6-311+G* basis set was used. For the heavier elements relativistic effects become important and cannot be neglected.[51,52] We therefore chose the relativistic pseudopotential (PP) approach[52] for Sb and Bi (denoted as R in front of all abbreviations). We believe that the error due to the neglect of relativistic effects would be larger than the error inherent in the pseudopotential approximation. For Bi we also applied a nonrelativistic pseudopotential in order to discuss relativistic effects. Relativistic effects for Sb and Bi are taken into account through the parametrization of the pseudopotential. Electron correlation was determined by second-order many-body perturbation theory (MP2).[50] This is an appropriate choice as a recent comparison between MP2 and configuration interaction calculations on main group element containing fluorides have shown that the two approaches lead to quite similar results for molecular properties.[49,53] However, nondynamic correlation effects become very important for the molecules inverting through T-shaped structures, and we have therefore performed small CASSCF/MP2 (abbreviated as CASPT2 for the following) calculations for NF_3 and PF_3 using the program package MOLCAS.[54] In these calculations the HOMO and the first seven LUMOs define the active space for the zeroth-order wave function. This results in 40 configuration-state functions (CSF) within the CASSCF procedure. This was the smallest common active space for all structures (C_{3v}, C_{2v}, and D_{3h}); *i.e.*, the orbitals change substantially from the ground state C_{3v} to the D_{3h} structure and switching of active with inactive orbitals has to be avoided. We did not consider lower lying occupied orbitals in the active CASSCF space because the number of determinants would become too large for a subsequent MP2 procedure. The geometry was optimized numerically at the CASPT2 level. The same basis sets as in the single-reference MP2 calculations were used, *i.e.*, a 6-2111+G* basis set for N and P[7] and a 6-311+G* basis set for F. For PF_3 this resulted in 160 primitive Gaussian functions contracted to 92 basis functions. The CASPT2 dipole moments for NF_3 and PF_3 were derived from the finite field approximation using electric fields of +0.002, +0.001, 0, −0.001, and −0.002 au in the direction of the C_3-axis.

Local density functional (LDA)[28] calculations were carried out using Baerends's ADF program,[55] Delley's DMOL,[37,56] and the density functional extension of GAUSSIAN92 code.[50] The various exchange-correlation functionals used are that of Slater[58] extended by Barth and Hedin,[59] Lee–Yang–Parr (LYP),[60] Vosko–Wilk–Nusair (VWN),[61] and Hedin–Lundquist (HL) (modified by Moruzzi, Janak, and Williams).[62] For NF_3 and PF_3 we have also investigated the influence of the nonlocal or inhomogeneous gradient correction to exchange by Becke (B),[57] Perdew's gradient-corrected correlation functional (P),[63] and Stoll's self-interaction correction (SIC).[64] The basis set used within DMOL was a double numerical basis with a polarization function (DNP) and a fine mesh for the numerical integration procedure (XFINE).[56] Vibrational frequencies were calculated using the finite difference method and the HL (DMOL) and VWN (Gaussian92/DFT) density functional. The ADF code was used to study the basis set effects on the optimized geometries, as this program can provide relatively large STO basis sets. The optimized triple-ζ Slater type basis sets (TZ) of Baerends *et al.* have been applied, augmented by one (TZP) or two (TZ2P) polarization functions.[65] The frozen atomic core approximation within the ADF code was used throughout. For the GAUSSIAN92/DFT package the GTO basis sets and pseudopotentials as described above have been used. A very tight grid for the numerical integration was chosen (96 radial shells around each atom: 32 θ points and 64 ϕ points) to avoid inaccuracies in the frequency calculation.

For further comparison, AM1[66] (NF_3 and PF_3), PM3[67] (all MF_3 species), and MNDO[68] (NF_3 and PF_3) calculations were carried out. These methods are among the most widely used semiempirical approximations in quantum chemistry, and they should be capable of describing the inversion behavior correctly. In particular, such semiempirical methods are expected to describe the symmetry breaking encountered for PF_3 to BiF_3 (but not for NF_3) correctly, at least at a qualitative level.

Two-dimensional inversion hypersurfaces $E(\alpha,\beta)$ were constructed by calculating pointwise the electronic energy and optimizing all M–F bond distances in MF_3. The angles α and β are defined as follows:

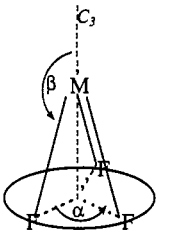

α denotes the F–M–C_3–F torsion angle (in the C_{3v} point group). β denotes the C_3–M–X inversion angle (β is 90° at the planar transition state). The covering group for the hypersurface is of C_s symmetry. This particular angle definition has the advantage that α is kept constant at 120° for the expected C_{3v} inversion path. Therefore, symmetry breaking away from the usual C_{3v} symmetry is determined merely by changing the angle α.

(45) Binning, R. C.; Curtiss, L. A. *J. Comput. Chem.* **1990**, *11*, 1207.
(46) Schneider, W.; Thiel, W.; Komornicki, A. *J. Phys. Chem.* **1990**, *94*, 2810.
(47) (a) Sakai, Y.; Miyoshi, E. *J. Chem. Phys.* **1988**, *89*, 4452. (b) Huzinaga, S.; Sakai, Y.; Miyoshi, E.; Narita, S. *J. Chem. Phys.* **1990**, *93*, 3319.
(48) Igel-Mann, G.; Flad, H. J.; Feller, C.; Preuss, H. *J. Mol. Struct. (THEOCHEM)* **1990**, *209*, 313.
(49) Schwerdtfeger, P.; Heath, G. A.; Dolg, M.; Bennett, M. A. *J. Am. Chem. Soc.* **1992**, *114*, 7518.
(50) Frisch, M. J.; Trucks, G. W.; Schlegel, H. B.; Gill, P. M. W.; Johnson, B. G.; Wong, J. B.; Foresman, J. B.; Robb, M. A.; Head-Gordon, M.; Replogle, E. S.; Gomperts, R.; Andres, J. L.; Raghavachari, K.; Binkley, J. S.; Gonzales, C.; Martin, R. L.; Fox, D. J.; DeFrees, D. J.; Baker, J.; Stewart, J. J. P.; Pople, J. A. *Program GAUSSIAN92/DFT*, Revision F.3; Gaussian Inc.: Pittsburgh, PA, 1993.
(51) Pyykkö, P. *Chem. Rev.* **1988**, *88*, 563.
(52) (a) Christiansen, P. A.; Ermler, W. C.; Pitzer, K. S. *Annu. Rev. Phys. Chem.* **1985**, *36*, 407. (b) Igel-Mann, G.; Stoll, H.; Preuss, H. *Mol. Phys.* **1988**, *65*, 1321. (c) Küchle, W.; Dolg, H.; Stoll, H.; Preuss, H. *Mol. Phys.* **1991**, *74*, 1245.
(53) (a) Schwerdtfeger, P.; Ischtwan, J. *J. Mol. Struct. (THEOCHEM)* **1994**, *306*, 9. (b) Schwerdtfeger, P.; Ischtwan, J. *J. Comput. Chem.* **1993**, *14*, 913.
(54) Andersson, K.; Blomberg, M.R.A.; Fülscher, M. P.; Kellö, V.; Lindh, R.; Malmqvist, P.-Aa.; Noga, J.; Olsen, J.; Roos, B. O.; Sadlej, A. J.; Siegbahn, P. E. M.; Urban, M.; Widmark, P.-O. *MOLCAS*, Version 2; University of Lund: Sweden 1991.
(55) (a) Baerends, E. J.; Ellis, D. E.; Ros, P. *Chem. Phys.* **1973**, *2*, 41. (b) Snijders, J. G.; Baerends, E. J. *Mol. Phys.* **1978**, *36*, 1789. (c) Snijders, J. G.; Baerends, E. J.; Ros, P. *Mol. Phys.* **1979**, *38*, 1909. (d) Ziegler, T.; Rauk, A. *Theor. Chim. Acta.* **1977**, *46*, 1. (e) Ziegler, T.; Snijders, J. G.; Baerends, E. J. *J. Chem. Phys.* **1981**, *74*, 1271.
(56) (a) *Program DMOL*, Version 2.3.0; Biosym Technologies: San Diego, 1993. (b) Delley, B. *Chem. Phys.* **1986**, *110*, 329. (c) Delley, B. *J. Chem. Phys.* **1990**, *92*, 508.
(57) Becke, A. D. *Phys. Rev. A* **1988**, *38*, 3098.
(58) Slater, J. C. *Phys. Rev.* **1971**, *81*, 385.
(59) Barth, U. v.; Hedin, L. *J. Phys. C* **1972**, *5*, 1629.
(60) Lee, C.; Yang, W.; Parr, R. G. *Phys. Rev. B* **1988**, *37*, 785.
(61) Vosko, S. H.; Wilk, L.; Nusair, M. *Can. J. Phys.* **1980**, *58*, 1200.
(62) (a) Hedin, L.; Lundquist, B. I. *J. Phys. C* **1971**, *4*, 2064. (b) Moruzzi, V. L.; Janak, J. F.; Williams, A. R. *Calculated Electronic Properties of Metals*; Pergamon: New York, 1978.
(63) (a) Perdew, J. P. *Phys. Rev. B* **1986**, *33*, 8822. (b) Perdew, J. P. *Electronic Structure of Solids*; Ziesche, P., Eschring, H., Eds.; Akademie: Berlin, 1991.
(64) (a) Stoll, H.; Golka-Pavlidou, C. M. E.; Preuss, H. *Theor. Chim. Acta* **1978**, *49*, 143. (b) Stoll, H.; Golka-Pavlidou, C. M. E.; Preuss, H. *Theor. Chim. Acta* **1980**, *55*, 29.
(65) Baerends, E. J.; Ros, P. *Int. J. Quantum Chem., Quantum Chem. Symp.* **1978**, No. 12, 169.
(66) Dewar, M. J. S.; Zoebisch, E. G.; Healy, E. F. *J. Am. Chem. Soc.* **1985**, *107*, 3902.
(67) Stewart, J. J. P. *J. Comput. Chem.* **1989**, *10*, 209.
(68) (a) Dewar, M. J. S.; Thiel, W. *J. Am. Chem. Soc.* **1977**, *99*, 4499. (b) Dewar, M. J. S.; McKee, M. L.; Rzepa, H. S. *J. Am. Chem. Soc.* **1978**, *100*, 3607.

Table 1. Molecular Properties for MF_3 Compounds (M = N to Bi) Determined *via* Various Methods[a]

		minimum			inversion point			
molecule	method	r_e	β_e	μ_e	r^a	r^e	α	E_a
NF_3	HF	1.321	115.4	0.29	1.305	1.305	120	325.8
	MP2	1.371	116.1	0.25	1.339	1.339	120	336.7
	CASPT2	1.376	115.6	0.41	1.335	1.335	120	299.1
	VWN	1.374	116.3	0.17	1.331	1.331	120	322.4
	AM1	1.360	115.7	0.04	1.366	1.366	120	447.2
	PM3	1.354	113.6	0.26	1.338	1.338	120	465.8
	MNDO	1.315	112.5	0.20	1.339	1.339	120	506.8
	exptl	1.365	115.9	0.24				
PF_3	HF	1.574	120.1	1.68	1.562	1.646	86.4	279.5
	MP2	1.607	119.8	1.67	1.598	1.678	87.8	222.1
	CASPT2	1.598	120.2	1.81	1.588	1.677	88.8	192.2
	VWN	1.609	120.2	1.55	1.605	1.680	87.7	184.5
	AM1	1.591	120.5	2.09	1.541	1.562	83.1	330.0
	PM3	1.558	121.0	2.26	1.555	1.609	83.0	270.2
	MNDO	1.556	118.7	2.44	1.547	1.595	90.2	342.1
	exptl	1.570	120.2	1.03				
AsF_3	HF	1.709	121.4	3.14	1.690	1.798	85.0	230.2
	MP2	1.748	120.9	3.00	1.735	1.830	86.9	185.3
	VWN	1.746	121.1	2.84	1.731	1.827	85.8	155.3
	PM3	1.706	120.9	2.50	1.699	1.727	78.0	264.8
	exptl	1.704	120.9	2.83				
SbF_3	RHF	1.864	122.3	4.37	1.848	1.938	83.0	184.0
	RMP2	1.903	121.7	4.16	1.891	1.972	84.9	151.3
	VWN	1.917	121.4	4.05	1.907	1.981	84.4	121.7
	PM3	1.953	125.1	5.53	1.953	1.978	77.4	191.5
	exptl	1.879	121.6					
BiF_3	HF	1.989	122.6	5.55	1.972	2.065	81.4	175.7
	MP2	2.025	122.1	5.23	2.011	2.098	83.2	152.0
	VWN	2.033	121.9	4.89	2.022	2.104	82.4	126.9
	RHF	2.001	121.3	6.71	1.978	2.099	87.2	148.6
	RMP2	2.050	120.4	6.13	2.018	2.127	89.9	132.9
	RVWN	2.053	120.4	5.64	2.120	2.120	120	104.7
	PM3	1.990	124.3	6.27	1.989	1.989	120	141.1

[a] M–F bond distances r in angstroms, angles α and β in degrees, and dipole moments μ_e in debye. r_e is the minimum bond distance, r^a and r^e are the axial and equatorial bond distances in the C_{2v} transition structure, respectively ($r^a = r^e$ for the D_{3h} geometry), β is the C_3–M–F angle, and α is the angle between the axial and equatorial M–F bonds. Experimental values from ref 69. For the LDA calculations the same GTO basis set has been used as in the HF calculations.

Each hypersurface consists of 1036 optimized points. We confirmed the local C_s symmetry of the inversion path by calculating the MEIP starting from the C_{2v} transition state for PF_3. We point out that the HF hypersurfaces presented in this work are useful only for qualitative discussions of the inversion process. Because of the inherent nature of the inversion process a multiconfiguration (MC) treatment would certainly be more appropriate, especially in the high-energy region of the potential energy surface. This was beyond our computational capability mainly because of the large numbers of points needed for constructing these hypersurfaces. We therefore restricted our investigations to HF ground state hypersurfaces only.

III. Results and Discussion

Molecular Properties. The calculated molecular properties of the group 15 fluorides MF_3 are listed in Tables 1–3. In a recent paper Breidung and Thiel[41] discussed the minimum structures of all group 15 halides in detail at the pseudopotential HF level, so we discuss only briefly the most important points. As expected, Hartree–Fock calculations underestimate the M–F bond distance, while the MP2 method seems to overestimate it. The LDA results using the VWN functional slightly overestimate the M–F bond distances (Table 1). This is in agreement with the LDA results reported by Delley,[37] who used a Hedin–Lundquist exchange correlation potential[62] for NF_3 and PF_3. CASPT2 improves the bond distance of PF_3 slightly compared to the single-reference MP2 treatment, and the CASPT2 bond angle of PF_3 is now almost identical to the experimental value. We mention, however, that the gas-phase structures of the heavier element containing fluorides

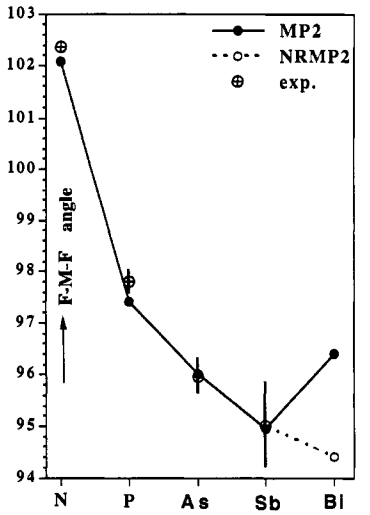

Figure 1. F–M–F minimum bond angles of group 15 fluorides; experimental values from ref 69. The experimental errors are indicated by bars.

(PF_3, AsF_3, and SbF_3) have not been measured accurately and uncertainties in bond lengths and bond angles can be as large as ±0.01 Å and ±0.8°.[69] The MP2 bond angles are in very good agreement with the experimental values, Figure 1.

A comparison of the molecular properties calculated at the HF level (Table 1) with the results of other authors shows values differing from those recently published by Huzinaga and co-workers.[41,47] For example, our Sb–F bond distance of SbF_3 at the pseudopotential HF level is 1.864 Å. Huzinaga *et al.*[47] obtain 1.885 Å within his model-potential approach, Breidung and Thiel[41] calculated 1.834 Å, and Dixon and Arduengo[11] obtain 1.874 Å in an all-electron calculation. Huzinaga *et al.* attribute their differences, compared to the work of Dixon and Arduengo, to the basis set superposition error (BSSE), which should be larger at the all-electron level compared to the simple model-potential approach. However, the symmetric Sb–F stretching force constant is quite large (~3.7 mdyn/Å; Table 4), and the BSSE should only lead to minor changes in the Sb–F bond distance. Moreover, taking into account that for antimony major relativistic effects are included by the pseudopotential adjustment, our Sb–F bond distance agrees quite well with the value of Dixon and Arduengo. We therefore conclude that the difference between our and Huzinaga's results is rather due to basis set incompleteness and the errors in the adjustment of the model potential. In contrast, our HF dipole moments agree quite well with Huzinaga's results (2.63 D for AsF_3 and 3.78 D for SbF_3),[47] but not with the results obtained by Breidung and Thiel at the pseudopotential HF level (3.14 D for AsF_3 and 4.79 D for SbF_3).[41] Breidung and Thiel's calculated HF dipole moments seem to be rather low, and therefore, their agreement with experimental results seems to be rather fortuitous. Our MP2 dipole moments are in reasonable

(69) (a) Sheridan, J.; Gordy, W. *Phys. Rev.* **1950**, *79*, 513. (b) Kisliuk, P. *J. Chem. Phys.* **1954**, *22*, 86. (c) Bartell, L. S.; Hirst, R. C. *J. Chem. Phys.* **1959**, *31*, 449. (d) McClellan, A. L. *Tables of Experimental Dipole Moments*; W. H. Freeman and Company: San Francisco, 1963. (e) Otake, M.; Matsumura, C.; Morino, Y. *J. Mol. Spectrosc.* **1968**, *28*, 316. (f) Morino, Y.; Kuchitsu, K.; Moritani, T. *Inorg. Chem.* **1969**, *8*, 867. (g) Konaka, S.; Kimura, M. *Bull. Chem. Soc. Jpn.* **1970**, *43*, 1693 and references therein. (h) Konaka, S. *Bull. Chem. Soc. Jpn.* **1970**, *43*, 3107. (i) Hirota, E.; Morino, Y. *J. Mol. Spectrosc.* **1970**, *33*, 460. (j) Chikaraishi, T.; Hirota, E. *Bull. Chem. Soc. Jpn.* **1973**, *46*, 2314. (k) Hellwege, K. H. *Landolt-Börnstein, Zahlenwerte und Funktionen aus Naturwissenschaften und Technik*; Springer: Berlin, 1976; Vol. 7. (l) Kawashima, Y.; Cox, A. P. *J. Mol. Spectrosc.* **1977**, *65*, 319. (m) Harmony, M. D.; Laurie, V. W.; Kuczkowski, R. L.; Schwendeman, R. H.; Ramsay, D. A.; Lovas, F. J.; Lafferty, W. J.; Maki, A. G. *J. Phys. Chem. Ref. Data* **1979**, *8*, 619.

(70) Hoskins, L. C.; Lord, R. C. *J. Chem. Phys.* **1965**, *43*, 155.

(71) Nakamoto, K. *Infrared and Raman Spectroscopy of Inorganic and Coordination Compounds*, 4th ed.; Wiley: New York, 1986.

(72) Corbridge, D. E. C. *Top. Phosphorus Chem.* **1969**, *6*, 235.

(73) Fischer, T. *Program MOLVIB*; ETH:Zürich, 1994.

Table 2. Molecular Properties for MF_3 Compounds (M = N to Bi) Determined *via* Different Density Functional Approximations[a]

			minimum			inversion point			
molecule	method	basis	r_e	β_e	μ_e	r^a	r^e	α	E_a
NF_3	VWN	DNP	1.394	116.7	0.13	1.346	1.346	120	328.3
	VWN	TZP	1.378	115.9	0.13	1.334	1.334	120	316.3
	VWN	TZ2P	1.369	115.8	0.12	1.326	1.326	120	311.8
	VWN	GTO	1.374	116.3	0.17	1.331	1.331	120	322.4
	VWN/B	TZP	1.440	115.9	0.38	1.379	1.379	120	325.2
	VWN/B	TZ2P	1.429	115.9	0.34	1.370	1.370	120	321.9
	VWN/B	GTO	1.427	116.2	0.37	1.376	1.376	120	331.0
	VWN/S	TZP	1.389	115.9	0.15	1.343	1.343	120	321.1
	VWN/S	TZ2P	1.380	115.8	0.14	1.336	1.336	120	316.0
	VWN/S+B	TZP	1.453	115.9	0.38	1.388	1.388	120	330.6
	VWN/S+B	TZ2P	1.443	115.9	0.37	1.380	1.380	120	326.4
	P/B	TZP	1.411	115.8	0.23	1.356	1.356	120	329.0
	P/B	TZ2P	1.401	115.8	0.22	1.349	1.349	120	325.0
	P/B	GTO	1.409	116.3	0.29	1.361	1.361	120	336.4
	LYP	GTO	1.371	116.4	0.16	1.330	1.330	120	326.3
	LYP/B	GTO	1.423	116.4	0.35	1.373	1.373	120	334.2
	HL	DNP	1.394	116.7	0.13	1.347	1.347	120	329.3
	HL/B	DNP	1.448	116.4	0.27	1.395	1.395	120	338.1
	exptl		1.365	115.9	0.24				
PF_3	VWN	DNP	1.613	120.2	1.17	1.612	1.673	87.8	169.0
	VWN	TZP	1.598	120.0	1.16	1.595	1.668	88.4	171.7
	VWN	TZ2P	1.578	119.9	1.05	1.574	1.656	88.2	187.8
	VWN	GTO	1.609	120.2	1.55	1.605	1.680	87.7	184.5
	VWN/S	TZP	1.610	120.0	1.19	1.607	1.681	88.5	168.1
	VWN/S	TZ2P	1.590	119.9	1.08	1.586	1.669	88.3	183.3
	VWN/S+B	TZP	1.656	118.3	1.37	1.639	1.752	90.9	166.1
	VWN/S+B	TZ2P	1.638	118.2	1.27	1.618	1.742	91.0	181.6
	VWN/B	TZP	1.643	118.3	1.34	1.626	1.737	90.6	170.4
	VWN/B	TZ2P	1.625	118.3	1.23	1.606	1.727	90.7	186.3
	VWN/B	GTO	1.645	119.6	1.78	1.637	1.730	88.7	179.0
	P/B	TZP	1.621	118.9	1.14	1.612	1.702	89.6	170.7
	P/B	TZ2P	1.601	119.0	1.05	1.591	1.691	89.5	186.5
	P/B	GTO	1.634	119.8	1.63	1.628	1.710	88.1	180.1
	LYP	GTO	1.607	120.3	1.53	1.605	1.674	87.4	181.5
	LYP/B	GTO	1.643	119.7	1.76	1.635	1.723	88.4	176.7
	HL	DNP	1.615	120.2	1.17	1.614	1.674	87.8	168.4
	HL/B	DNP	1.653	119.3	1.33	1.649	1.728	88.9	166.2
	exptl		1.570	120.2	1.03				
AsF_3	VWN	DNP	1.737	121.0	2.47	1.726	1.814	86.5	155.7
	VWN	TZP	1.711	121.0	2.38	1.700	1.802	87.2	159.1
	VWN	TZ2P	1.702	121.0	2.32	1.689	1.795	87.0	169.9
	VWN	GTO	1.746	121.1	2.84	1.731	1.827	85.8	155.3
	VWN/S	TZP	1.724	120.9	2.38	1.713	1.815	87.6	155.7
	VWN/S	TZ2P	1.712	121.0	2.32	1.700	1.806	87.2	166.7
	VWN/S+B	TZP	1.779	119.9	2.72	1.762	1.888	89.6	146.6
	VWN/S+B	TZ2P	1.771	119.6	2.63	1.752	1.882	89.8	156.2
	VWN/B	TZP	1.764	120.1	2.71	1.748	1.872	89.3	150.5
	VWN/B	TZ2P	1.757	119.8	2.62	1.738	1.866	89.5	160.0
	P/B	TZP	1.741	120.4	2.46	1.728	1.841	88.3	155.1
	P/B	TZ2P	1.732	120.3	2.39	1.716	1.833	88.2	164.8
	HL	DNP	1.738	121.0	2.47	1.729	1.816	86.5	155.2
	HL/B	DNP	1.788	120.0	2.66	1.780	1.884	88.6	146.0
	exptl		1.704	120.9	2.83				
SbF_3	VWN	DNP	1.915	122.1	3.43	1.907	1.978	83.7	129.6
	VWN	GTO	1.917	121.4	4.05	1.907	1.981	84.4	121.7
	HL	DNP	1.917	122.1	3.44	1.906	1.980	83.7	129.4
	HL/B	DNP	1.969	121.0	3.62	1.964	2.048	85.8	124.3
	exptl		1.879	121.6					

[a] M–F bond distances r in angstroms, angles α and β in degrees, and dipole moments μ_e in debye. r_e is the minimum bond distance, r^a and r^e are the axial and equatorial bond distances in the C_{2v} transition structure, respectively ($r^a = r^e$ for the D_{3h} geometry), β is the C_3–M–F angle, and α is the angle between the axial and equatorial M–F bonds. VWN denotes the Vosko–Wilk–Nusair functional, P the Perdew gradient-corrected functional, LYP the gradient-corrected Lee–Yang–Parr functional, HD the Hedin–Lundquist functional, B the Becke correction, S the Stoll self-interaction correction, DNP the double numerical basis set using DMOL, and TZ the triple-ζ basis set using ADF; P and 2P indicate one or two polarization functions added, respectively. For BiF_3 see Table 1. The ADF TZP calculations for the transition state of SbF_3 did not converge. Experimental values from ref 69.

agreement with the available experimental values with the exception of PF_3 (Table 1). Recent results by Sadlej *et al.*[43] using a very large basis set indicate that the experimental dipole moment of PF_3 (Table 1) is correct. However, our CASPT2 polarizability $\alpha^{\parallel}$ is 20 au, which is in reasonable agreement with the result of Sadlej *et al.*[43] (21 au). We attribute the error in the MP2 and CASPT2 dipole moment of PF_3 as being due to deficiencies in the phosphorus 6-2111+G* basis set (derived from the standard 6-311+G* basis set). These effects are either less important or self-canceling when we calculate the polarizability. For NF_3 we obtain a smaller value for CASPT2 polarizability $\alpha^{\parallel}$ as expected (13 au). Mack and Oberhammer[34] reported HF as well as MP2 6-31G** results for NF_3. Considering the different basis sets used in our work, their values (HF, r_e = 1.328, β_e = 116.5; MP2, r_e = 1.385, β_e = 115.6, μ = 0.39 D) are in good agreement with ours.

Table 3. HF, MP2, LDA, AM1, PM3, and MNDO Harmonic Frequencies[a]

molecule	method	$\nu_1(A_1)$	$\nu_2(A_1) = \nu_0$	$\nu_3(E)$	$\nu_4(E)$	$\Delta\nu$
NF_3	HF	1236(48)	769(9)	1218(250)	594(0.4)	180
	MP2	1059(45)	670(3)	936(234)	505(0.7)	19
	VWN	1041(46)	647(2)	860(285)	482(3)	19
	VWN/B	953(46)	565(1)	737(260)	422(8)	104
	P/B	992(47)	596(1)	786(273)	444(6)	69
	LYP	1047(44)	653(2)	872(285)	486(2)	17
	LYP/B	963(45)	573(1)	754(264)	429(7)	46
	HL/DNP	1030	618	870	462	29
	AM1	1270(23)	610(18)	1303(107)	453(2)	179
	PM3	1140(14)	583(16)	1189(125)	462(5)	122
	MNDO	1436(46)	781(41)	1528(168)	589(5)	310
	exptl	1035	649	910	500	
PF_3	HF	938(198)	519(47)	899(247)	372(8)	36
	MP2	861(161)	469(32)	824(228)	336(6)	24
	VWN	844	437(25)	813(202)	310(5)	45
	VWN/B	777(136)	415(20)	737(205)	298(4)	89
	P/B	799(134)	419(22)	766(202)	300(5)	75
	LYP	848(136)	435(25)	819(199)	309(5)	43
	LYP/B	782(133)	413(20)	744(203)	296(4)	65
	HL/DNP	839	421	825	301	50
	AM1	1076(23)	382(43)	1073(96)	295(9)	139
	PM3	790(92)	335(39)	759(177)	251(8)	112
	MNDO	1103(65)	472(66)	1089(165)	368(13)	120
	exptl	893	487	858	346	
AsF_3	HF	767(105)	367(43)	768(159)	283(8)	58
	MP2	699(76)	325(28)	667(138)	254(6)	23
	VWN	697(65)	314(21)	665(124)	238(5)	31
	HL/DNP	708	304	676	233	29
	PM3	741(89)	290(33)	764(25)	245(8)	53
	exptl	739	337	699	262	
SbF_3	HF	696(97)	289(49)	670(127)	225(9)	33
	MP2	636(71)	257(35)	617(109)	204(7)	8
	VWN	622(60)	225(26)	606(98)	178(6)	29
	HL/DNP	643	220	628	175	22
	PM3	733(26)	232(26)	701(57)	205(7)	47
	ref 41[c]	659	275	632	213	
	exptl	654	259	624	(210)[b]	
BiF_3	HF	655(81)	237(48)	634(113)	191(9)	
	MP2	600(56)	217(35)	586(92)	179(7)	
	VWN	590(46)	197(26)	577(83)	163(6)	
	RHF	625(87)	215(35)	601(131)	182(9)	
	RMP2	580(52)	189(27)	559(104)	164(7)	
	RVWN	575(41)	175(21)	555(92)	149(5)	
	PM3	675(15)	190(21)	655(39)	180(5)	
	ref 41[c]	618	234	595	192	

[a] ν (cm^{-1}), infrared intensities in 10^3 m/mol (set in parentheses after the wavenumbers) for the MF_3 compounds (M = N to Bi) in C_{3v} symmetry. If not otherwise indicated, HF and MP2 refer to NRHF and NRMP2, respectively. Experimental values from refs 70–72. $\Delta\nu$ is the mean deviation from the experimental result (in cm^{-1}). For the LDA calculations the HL parametrization within DMOL and the VWN/GTO with and without the Becke correction has been used. [b] Estimated value for SbF_3 using a comparison between the MP2 and experimental frequencies of NF_3, PF_3, and AsF_3. [c] Breidung and Thiel's predicted frequencies using a scaling procedure.

Table 4. MP2 Harmonic Valence Force Field in Symmetry Coordinates for the Group 15 Fluorides[a]

molecule	method	k_r	k_α	$k_{rr'}$	$k_{\alpha\alpha'}$	$k_{r\alpha}$	$k'_{r\alpha}$
NF_3	MP2	0.286	0.480	0.055	0.070	0.054	–0.001
PF_3	MP2	0.309	0.341	0.021	0.060	0.018	–0.003
AsF_3	MP2	0.263	0.251	0.013	0.037	0.002	–0.002
SbF_3	RMP2	0.240	0.202	0.007	0.031	–0.004	–0.0004
BiF_3	NRMP2	0.229	0.180	0.005	0.026	–0.008	0.0007
	RMP2	0.210	0.151	0.007	0.020	–0.013	–0.0002

[a] Units in au and rad. $k'_{r\alpha}$ is the off-diagonal force constant between the M–F bond and the adjacent FMF plane.

Table 2 contains results using different local density approximations. Versluis and Ziegler[36] reported LDA calculations using triple-ζ STO basis sets augmented by two d-polarization functions (TZ2P). Their calculations were of Hartree–Fock–Slater type (HFS), and it may be useful to compare these with our LDA results (see Tables 1 and 2): r_e = 1.390 Å and β_e = 116.3° for NF_3; r_e = 1.559 Å, β_e = 120.1° for PF_3 at the HFS level.[36] The VWN functional using the same TZ2P basis set performs slightly better than HFS (Table 2). We note some general trends: The Becke gradient correction increases the M–F bond distances significantly, resulting in relatively large deviations from experimental results. For example, the experimental P–F bond length in PF_3 is 1.570 Å. VWN is close to this value (1.578 Å using the TZ2P basis set). The Becke gradient correction to the exchange functional increases the bond distance to 1.625 Å. The Perdew correction to the correlation functional slightly corrects this error (1.601 Å for P/B; see Table 2). The Stoll SIC correction[64] leads to a further increase in the P–F bond distance (1.638 Å with VWN/S+B and TZ2P). A similar picture is obtained for the other fluorides. The HL, VWN, and LYP functionals seem to perform equally well as also found by Johnson *et al.*[33] Comparing the different basis sets used in the LDA calculations we conclude that the TZ2P basis set performs extremely well compared to the standard GTO and DNP basis sets used in the other programs. Since in LDA the computation of a large number of two-electron integrals is avoided, reducing the computational cost from a maximum $\sim N^4$ to $\sim N^3$, we feel that the use of STO basis sets is a better choice. However, GTO basis sets are certainly useful to directly compare *ab-initio* with LDA results.

The three semiempirical methods (AM1, PM3, and MNDO) yield reasonable results for the molecular geometry. AM1 and PM3 seem to be superior to MNDO. The semiempirically calculated dipole moments for PF_3 are overestimated when compared with the experimental result. However, all semiempirical methods are able to account for the symmetry breaking of the inversion state in PF_3.

Table 3 shows that HF (harmonic) frequencies are overestimated relative to the experimental (fundamental) frequencies. The calculated MP2 frequencies are in excellent agreement with experimental values; the mean deviation $\Delta\nu$ varies only between 8 and 24 cm^{-1}, depending on the molecule. This result seems to be surprising if we consider that different basis sets have been used and that large deviations in the MP2 frequencies were recently reported for group 15 hydrides.[7] It gives, however, confidence for the prediction of the vibrational spectrum of BiF_3; *i.e.*, the MP2 values listed in Table 3 should not deviate too much from experimental measurements. Note, however, that anharmonicity effects are not included in our calculations and a direct comparison with experimental frequencies should not be overemphasized. However, such effects should not contribute to $\Delta\nu$ by more than 20 cm^{-1}. We also estimate the yet to be measured SbF_3 $\nu_4(E)$ mode which should be observed at around 210 cm^{-1}. In Table 3 we included the predictions of the vibrational spectra of SbF_3 and BiF_3 published recently by Breidung and Thiel.[42] Their SbF_3 $\nu_4(E)$ mode is in good agreement with our predicted value; however, the $\nu_2(A_1)$ mode of BiF_3 is markedly different from our MP2 value. Mack and Oberhammer[34] reported MP2 frequencies for NF_3 which are close to our values. Breidung and Thiel[42] reported HF calculations for PF_3 [wavenumbers in cm^{-1}, intensities in parentheses in km/mol: $\nu_1(A_1)$ = 976(167), $\nu_2(A_1)$ = 513(42), $\nu_3(E)$ = 956(420), $\nu_4(E)$ = 364(13)]. They used a limited basis set (6-31G*), and a comparison to our HF values (Table 2) demonstrates that extension of the basis set can lead to relatively large changes in vibrational frequencies. The use of scaling factors[42] to obtain reasonable frequencies is therefore rather limited to the specific basis set applied. Binning and Curtiss[45] as well Schneider *et al.*[46] reported HF frequencies of AsF_3 which are in satisfactory agreement with our results. The density functionals perform reasonably well if the Becke correction is not included. However, the calculated frequencies are not as accurate as the MP2 results. This is in sharp contrast to the results recently obtained by Johnson *et al.* for quite a large number of molecules.[33] We feel that the Becke correction does not lead to acceptable results for the harmonic frequencies of NF_3 and PF_3 in contrast

Table 5. Molecular Properties for MF_2 ($^2B_1$) and MF ($^3\Sigma^-$) Compounds (M = N to Bi)[a]

molecule	method	r_e	γ_e	μ_e	ΔU_0	Δ_{corr}
		Group 15 Difluorides				
NF_2	HF	1.309	103.59	0.33	27.9	
	MP2	1.346	103.62	0.21	239.3	211
PF_2	HF	1.593	97.48	1.80	331.7	
	MP2	1.626	98.19	1.71	509.2	178
AsF_2	HF	1.732	95.48	2.96	278.6	
	MP2	1.769	96.79	2.76	458.6	180
SbF_2	RHF	1.888	93.97	3.90	292.9	
	RMP2	1.926	95.06	3.71	475.3	182
BiF_2	RHF	2.026	95.79	5.82	251.0	
	RMP2	2.059	96.93	5.32	440.8	190
	HF	2.012	93.25	4.76	294.5	
	MP2	2.047	94.22	4.51	474.4	180
		Group 15 Monofluorides				
NF	HF	1.296		−0.31	230.9	
	MP2	1.319		−0.10	374.6	144
	exptl	1.317				
PF	HF	1.612		1.52	767.8	
	MP2	1.643		1.49	834.7	67
	exptl	1.590				
AsF	HF	1.754		2.36	670.3	
	MP2	1.788		2.24	740.3	70
	exptl	1.736				
SbF	HF	1.912		2.96	699.9	
	MP2	1.949		2.88	770.2	70
	exptl	1.918				
BiF	RHF	2.051		4.41	620.4	
	RMP2	2.080		4.06	709.8	89
	HF	2.035		3.50	701.5	
	MP2	2.070		3.38	770.4	69
	exptl	2.052				

[a] M–F bond distances r_e in angstroms, angles γ_e in degrees, dipole moments μ_e in debye, decomposition energies ΔU_0 in kJ/mol ($MF_3 \rightarrow MF_2 + F$ for MF_2 and $MF_3 \rightarrow MF + F_2$ for MF). See text for the discussion of the dissociation limit. Experimental values from ref 74.

to the group 15 hydrides where the MP2 approximation does not perform well and density functional theory seems to perform much better.[7,33] Hence, the statement that current density functionals perform better than MP2[33] cannot be generalized. The semiempirical methods perform less well as can be seen by comparing the mean deviations $\Delta\nu$ for the different methods. The HF, MP2, and LDA infrared intensities are of similar magnitude. It is notable that the intensity of the $\nu_1(A_1)$ and $\nu_3(E)$ modes decreases from PF_3 to BiF_3 while the other two modes $\nu_2(A_1)$ and $\nu_4(E)$ do not change much between the different molecules. NF_3 seems to be an exception with relatively weak $\nu_1(A_1)$ and $\nu_2(A_1)$ modes.

Table 4 lists the force constants in symmetry coordinates. All off-diagonal force constants are small, indicating a good choice of internal coordinates. We note that $k_r(N-F) < k_r(P-F)$, in agreement with the relatively small decomposition energy of NF_3 ($\rightarrow NF + F_2$) relative to PF_3 (Table 5). This anomaly is not observed for the group 13 fluorides.[49]

Baechler *et al.*[4] noted that the inversion barriers E_a of nitrogen- and arsenic-containing compounds are very sensitive to the nature of the ligand. A comparison of the inversion barrier heights for the group 15 hydrides and fluorides, Figure 2A, indicates that the barrier height is very ligand sensitive for nitrogen. For As and Sb the inversion barriers of the hydrides and fluorides are of similar size. Note that E_a for SbF_3 and BiF_3 are *below* those of the corresponding hydrides (see also ref 11), contradicting ligand electronegativity arguments widely used.[25,26] Our results indicate that the inversion barriers of the group 15 fluorides decrease monotonically from N to Bi in contrast to Marynick's earlier suggestion.[14] Dixon and Arduengo demonstrated that successive substitution of the H ligand by F, *i.e.*, going from PH_3 to PH_2F, PHF_2, and finally PF_3, increases the barrier height. Figure 2A suggests that only small changes or even a reverse trend should be observed in the case of Sb and Bi.

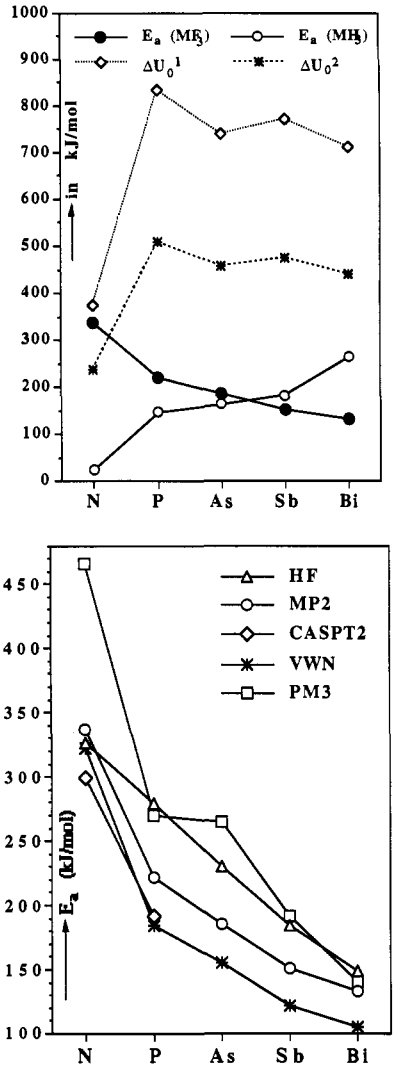

Figure 2. Inversion barriers of group 15 compounds. (A) MP2 inversion barriers E_a for the group 15 fluorides and hydrides and decomposition energies ΔU_0 for the group 15 fluorides. ΔU_0^1 is defined as ΔU_0·($MF_3 \rightarrow MF+F_2$) and ΔU_0^2 as $\Delta U_0(MF_3 \rightarrow MF_2+F)$. For the MF molecules the $^3\Sigma^-$ ground state has been chosen as the reference state (see text). (B) Inversion barriers E_a for the group 15 fluorides using different levels of approximation.

The calculated transition-state structures are in good agreement with previous results obtained by Dixon and Arduengo[9,11,12] as well as Edgecombe.[17] For example, Edgecombe obtained the following HF values for PF_3 using a 6-311G** basis set: r^e = 1.550 Å, r^a = 1.622 Å, α = 86.4°, E_a = 289 kJ/mol. These are close to our results (Table 1). The results from LDA compare quite well with the MP2 values for NF_3; however, for the heavier fluorides the LDA inversion barrier is consistently ca. 30 kJ/mol below the MP2 results and in the case of PF_3 close to the CASPT2 value, Figure 2B. The activation barrier seems to be relatively insensitive to the functional or basis set chosen; *i.e.*, we have E_a = 325 ± 15 kJ/mol for NF_3 and E_a = 177 ± 11 kJ/mol for PF_3 (Table 2). The F–M–F angle α, however, is quite sensitive to the LDA chosen; *i.e.*, for PF_3 α varies from ca. 88° (HL) to around 91° (VWN/B). This is as expected because the second-order JT distortion is sensitive to correlation effects. For example, the Perdew gradient correction to the correlation functional using the TZ2P basis set for PF_3 decreases the angle α from 90.7° to 89.5°, which is now in better agreement with the CASPT2 value of 88.8°. The semiempirical methods seem to overestimate the inversion barrier (especially in the case of NF_3, Figure 2B) and underestimate the F–M–F angle α (except for BiF_3, Table 1).

BiF_3 shows a very large relativistic change in the F–Bi–F angle of the planar transition-state structure ($\Delta_R\alpha = \alpha^{NR} - \alpha^R = -6.7°$

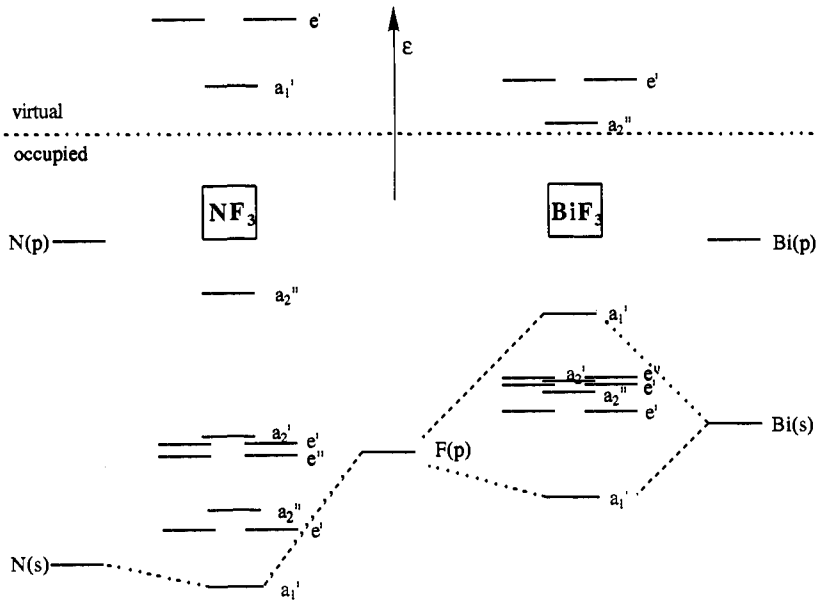

Figure 3. Qualitative MO-interaction schemes for NF_3 and BiF_3 at the trigonal planar D_{3h} structure.

at the MP2 level). This is also the case for the minimum angle β_e(MP2 $\Delta_R\beta_e = -1.7°$). This changes the trend in the F–M–F bond angles, which was expected to decrease down the group 15 series of compounds analogous to the group 15 hydrides,[7] *i.e.*, $NF_3 > PF_3 > AsF_3 > SbF_3 > BiF_3$. Figure 1 shows that this trend is valid if the nonrelativistic value for the F–Bi–F angle is taken instead of the relativistic one. Hence, this anomaly is a relativistic effect, and it would be interesting if this can be verified by experiment. In contrast, the Bi–F bond distance changes only slightly due to relativistic effects (MP2 $\Delta_R r_e = -0.013$ Å). We also note a large relativistic change in the BiF_3 dipole moment, *i.e.*, $\Delta_R\mu_e = -0.9$ D at the MP2 level and –0.75 D at the VWN level.

In Table 5 molecular properties of diatomic and triatomic group 15 fluorides MF and MF_2 are listed. Experimental values for the diatomic group 15 fluorides are available,[74] and these compare well with our calculated results. For the triatomic species, however, the gas-phase structures are not available. There seems to be no theoretical data available for AsF_2, SbF_2, and BiF_2, and only NF_2 and PF_2 have been studied by MCSCF or CI methods. Peterson *et al.*[75] obtained $r_e = 1.346$ Å and $\alpha_e = 103.2°$ for NF_2 using a CASSCF procedure, which is in good agreement with our results. Schaefer *et al.*[76] obtained $r_e = 1.581$ Å and $\alpha_e = 97.6°$ for PF_2 using a CISD procedure. Their results are in less agreement with our MP2 values. It is interesting that electron correlation contributions to the decomposition energies of MF_3 compounds vary only slightly from PF_3 to BiF_3, Table 5. NF_3 seems to be the exception, having unusually high correlation contributions. Finally, we mention the relatively low stability of NF_3 compared to the other group 15 fluorides (compare the ΔU_0 values of the decomposition reaction $MF_3 \rightarrow MF + F_2$ in Table 5). This is theoretical evidence for the known reduced stability of the oxidation state III relative to I for NF_3 when compared to the other group 15 fluorides. A similar trend is found in the higher oxidation state V compared to III; *i.e.*, NF_5 is an unknown species. This distinguishes the group 15 compounds from the group 13 compounds where the stability of the higher oxidation state decreases monotonically from BF_3 to TlF_3.

Frontier Orbitals and Second-Order Jahn-Teller Distortions. Marynick pointed out that the HOMO of group 15 compounds MX_3 in the trigonal planar arrangement (D_{3h}) is of either a_2'' (*e.g.*, NH_3, NF_3) or a_1' symmetry (*e.g.*, PF_3).[14-16] A qualitative MO picture is given in Figure 3 for the molecules NF_3 and BiF_3. It is well-known that the valence s-ionization potential and the s–p energy gap are unusually high for nitrogen compared to all the other group 15 atoms.[49,77] Hence, the N(2s) orbital is low in energy in contrast to the Bi(6s) orbital, which lies in the same region as the F(2p) orbitals. As a result, the N(2s) orbital does not mix strongly with the F(2p) orbitals and the low-lying a_1 orbital (a_1' in D_{3h} symmetry) of NF_3 is mainly of N(2s) character. This is not the case for BiF_3 (Figure 3) and for the other group 15 fluorides PF_3, AsF_3, and SbF_3. However, this does not explain the sudden change in the HOMO symmetry from NF_3 to PF_3.

Nitrogen is the most electronegative atom within the group 15 series of elements. As a consequence, the charge separation between N and F is relatively small in contrast to the other group 15 fluorides, which is reflected in the MF_3 dipole moments (Table 1) and the Mulliken atomic charges (Table 6). Hence, the main difference between NF_3 on the one side and the remaining group 15 fluorides PF_3, AsF_3, SbF_3, and BiF_3 on the other side is that the N–F bond is less ionic (therefore more covalent) compared to the heavier MF_3 species. A Mulliken population analysis (Table 6) demonstrates that for the heavier MF_3 compounds the density shift from the central atom to the fluorine ligand originates almost entirely from the M(p) and not from the M(s) orbitals. Depopulating central atom p orbitals in favor of F(p) orbitals *destabilizes* the a_2'' orbital (mainly M(p) character) and *stabilizes* the a_1' orbital (mainly F(p) character) in the trigonal planar arrangement, and this may rationalize the change in the HOMO symmetry from NF_3 to PF_3. This is reflected in the very different p populations at the inversion point (Table 6). As can be seen, the central atom p_z population (z-axis defined parallel to the C_3-axis) changes dramatically from NF_3 to the other group 15 fluorides. The order of orbital occupation is therefore sensitive to the difference in electronegativity between the central atom M and the ligand F. This implies that the change in orbital symmetry is more or less restricted to electronegative ligands, and it would be interesting to study the inversion barriers of the less electronegative halide ligands Cl, Br, and I.

(74) (a) Huber, K. P.; Herzberg, G. *Molecular Spectra and Molecular Structure, Vol. IV, Constants of Diatomic Molecules*; Van Nostrand Reinhold: New York, 1979. (b) Jones, W. E.; McLean, T. D. *J. Mol. Spectrosc.* **1981**, *90*, 481.
(75) Peterson, K. A.; Mayrhofer, R. C.; Woods, R. C. *J. Chem. Phys.* **1990**, *93*, 5020.
(76) Jim, S.; Colegrave, B. T.; Schaefer, H. F. *Inorg. Chem.* **1991**, *30*, 2969.
(77) Nyholm, R. S. *Proc. Chem. Soc.* **1961**, 273.
(78) Cherry, W.; Epiotis, N.; Borden, W. T. *Acc. Chem. Res.* **1977**, *10*, 167.

Table 6. HF and MP2 Mulliken Orbital Populations n_s and n_p and Gross Metal Charges q for the Group 15 Fluorides[a]

		minimum				inversion point			
	method	n_s	n_{p_z}	n_p	q	n_s	n_{p_z}	n_p	q
N	HF	1.98	1.26	2.82	0.12	1.38	2.07	3.61	−0.15
	MP2	1.92	1.32	2.88	0.04	1.41	2.05	3.64	−0.21
	VWN	2.00	1.32	2.96	−0.11	1.37	2.07	3.77	−0.29
P	HF	1.62	0.86	1.74	1.21	2.23	0.23	1.49	0.80
	MP2	1.78	0.84	1.85	0.93	2.25	0.41	1.62	0.66
	VWN	1.74	0.82	1.92	0.92	2.33	0.48	1.73	0.54
As	HF	1.74	0.79	1.63	1.29	2.02	0.42	1.34	1.24
	MP2	1.82	0.78	1.76	1.08	2.04	0.51	1.55	1.00
	VWN	1.86	0.76	1.86	0.93	2.08	0.66	1.69	0.83
Sb	RHF	2.18	0.68	1.34	1.26	2.12	0.18	1.22	1.37
	RMP2	2.20	0.67	1.48	1.07	2.09	0.29	1.49	1.16
	RVWN	2.24	0.66	1.58	0.94	2.21	0.38	1.52	1.01
Bi	HF	2.03	0.66	1.18	1.74	2.06	0.15	1.05	1.82
	MP2	2.06	0.66	1.33	1.53	2.07	0.26	1.24	1.58
	VWN	2.10	0.66	1.47	1.37	2.13	0.37	1.42	1.38
	RHF	2.07	0.56	1.11	1.80	2.07	0.15	0.98	1.91
	RMP2	2.07	0.59	1.32	1.56	2.08	0.27	1.22	1.64
	RVWN	2.06	0.62	1.51	1.38	2.18	0.38	1.39	1.38

[a] For the inversion point the molecule is defined in the xy-plane. The C_3 axis is defined in z-direction.

Unusual structures can often be explained by perturbation theory, using the distortion coordinates in the power expansion. This results in first-order and higher order corrections to the total electronic energy at the undistorted geometry, which are often referred to as the (static) first-order JT term, second-order (or pseudo) JT term, *etc.* Levin[5] presented Walsh diagrams for the inversion mode of trigonal pyramidal molecules such as NH_3 and explained the symmetry breaking of the trigonal planar D_{3h} structure as being due to a second-order JT distortion. In this case the a_2'' HOMO interacts with the a_1' LUMO ($a_2'' \otimes a_1'$), resulting in a distortion along the a_2'' mode. Levin also demonstrated that the energy gap between the two orbitals in the trigonal planar transition state is smaller in PH_3 when compared with NH_3 and, therefore, PH_3 has a higher inversion barrier than NH_3.[5] A more detailed discussion using frontier orbital theory can be found in ref 77. The second-order JT distortion can nicely explain the trend in the increasing barrier heights down the group 15 series of hydrides, as has been shown recently by one of us.[7] It is therefore interesting if a similar frontier orbital model can be used to explain trends of inversion properties of group 15 fluorides.

Let us discuss the distortion from the trigonal planar arrangement (D_{3h} symmetry) to the C_{3v} minimum structure. Table 7 lists the orbital energies for all the group 15 fluorides in the trigonal planar arrangement. Because of the second-order $a_2''_{HOMO} \otimes a_1'_{LUMO}$ JT mixing, the orbital-energy difference $\Delta\epsilon$ between the a_2'' HOMO and the a_1' LUMO ($\Delta\epsilon(NF_3) \ll \Delta\epsilon(PF_3)$) rationalizes the decrease in the inversion barrier from NF_3 to PF_3. However, the heavier fluorides do not show a similar clear trend. Moreover, one has to consider all the important contributions to the second-order JT term which are responsible for the distortion from D_{3h} into C_{3v} symmetry. Hence, frontier orbital theory does not seem to be very useful in explaining the overall trend in the inversion barriers. A more complex approach appears to be requisite using information from many electronically excited states to obtain accurate second-order JT matrix elements, which, however, would be computationally quite demanding. We also point out that NF_3^+ is more planar than neutral NF_3, *i.e.*, $\beta(NF_3^+) = 104.7° < \beta(NF_3) = 115.9°$ ($\beta = 90°$ at the trigonal planar geometry).[79] Here, the a_2'' orbital of NF_3^+ is only singly occupied, and we expect the second-order JT effect to be diminished for NF_3^+ compared to NF_3.

The MO scheme in Figure 4 shows the partition of the two irreducible representations (IRREP) for the a_2'' and a_1' HOMO of D_{3h} symmetry into point groups of lower symmetry (C_{3v}, C_{2v}, and C_s), which is important for further discussion of the inversion process. As can be seen, the a_1 orbital can transform into either an a_1' or an a_2'' orbital when moving toward local D_{3h} symmetry along the C_{3v} inversion path. Figure 4 also shows three-dimensional surfaces for the important orbitals involved in the inversion process. As mentioned above, in the C_{3v} process (*e.g.*, all group 15 hydrides)[7] the a_2'' orbital is the HOMO and the a_1' orbital the LUMO in the trigonal planar arrangement. Such molecules prefer an "a_2'' inversion" through a D_{3h} transition state. However, this sequence is inverted for the molecules PF_3, AsF_3, SbF_3, and BiF_3 (Table 5), and the orbital configuration becomes

(79) Curtiss, L. A. *Chem. Phys. Lett.* **1987**, *136*, 101.

Table 7. HF Orbital Energies of the Group 15 Fluorides at the D_{3h} Point at the Hypersurface (in au)[a]

		orbital energies	$\Delta\epsilon$
NF_3	occ	a_1' −1.085, e' −0.871, a_2'' −0.856, e'' −0.745, e' −0.725, a_2' −0.704, a_2'' −0.413	
	unocc	a_1' 0.083, e' 0.143, a_2'' 0.161	1.23
PF_3	occ	a_1' −0.921, e' −0.776, a_2'' −0.710, e' −0.694, e'' −0.670, a_2' −0.664, a_1' −0.399	
	unocc	a_2'' −0.056, a_1' 0.076, e' 0.077	0.48
AsF_3	occ	a_1' −0.893, e' −0.729, a_2'' −0.672, e' −0.659, e'' −0.642, a_2' −0.641, a_1' −0.435	
	unocc	a_2'' −0.079, a_1' 0.044, e' 0.047	0.48
SbF_3	occ	a_1' −0.813, e' −0.692, a_2'' −0.645, e' −0.636, e'' −0.624, a_2' −0.692, a_1' −0.419	
R	unocc	a_2'' −0.083, a_1' 0.028, e' 0.043	0.46
BiF_3	occ	a_1' −0.838, e' −0.651, a_2'' −0.612, e' −0.600, a_2' −0.597, e'' −0.594, a_1' −0.470	
R	unocc	a_2'' −0.086, a_1' 0.023, e' 0.035	0.51
BiF_3	occ	a_1' −0.712, e' −0.662, a_2'' −0.621, e' −0.611, a_2' −0.605, e'' −0.604, a_1' −0.410	
	unocc	a_2'' −0.071, a_1' 0.027, e' 0.034	0.44

[a] Only the first three LUMOs are shown. The orbital energy difference $\Delta\epsilon$ refers to the a_1' HOMO and the e' LUMO.

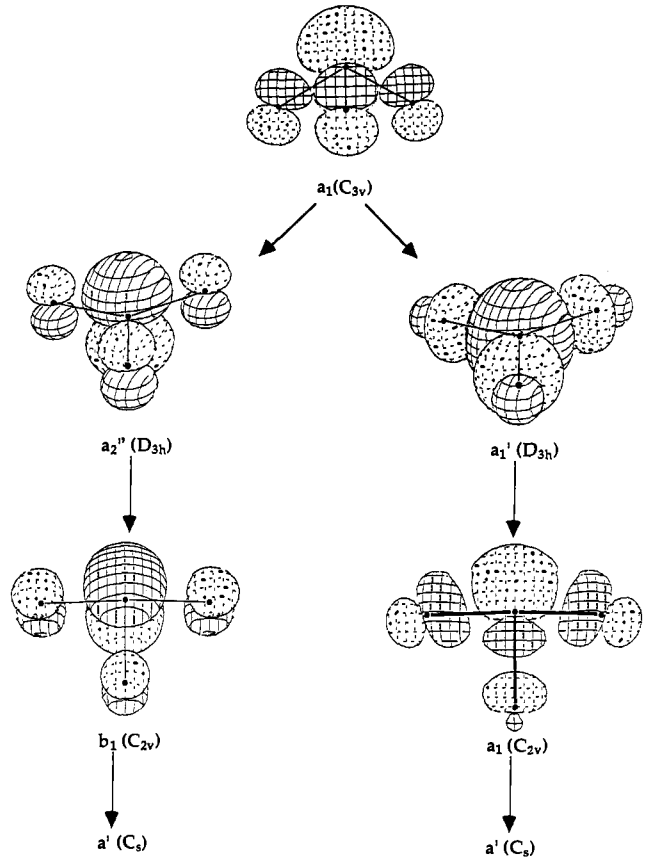

Figure 4. Qualitative MO plots at some important points at the (α,β)-inversion potential energy surface: (a, left) $C_{3v}(a_1) \rightarrow D_{3h}(a_2'') \rightarrow C_{2v}(b_1)$; (b, right) $C_{3v}(a_1) \rightarrow D_{3h}(a_1') \rightarrow C_{2v}(a_1)$.

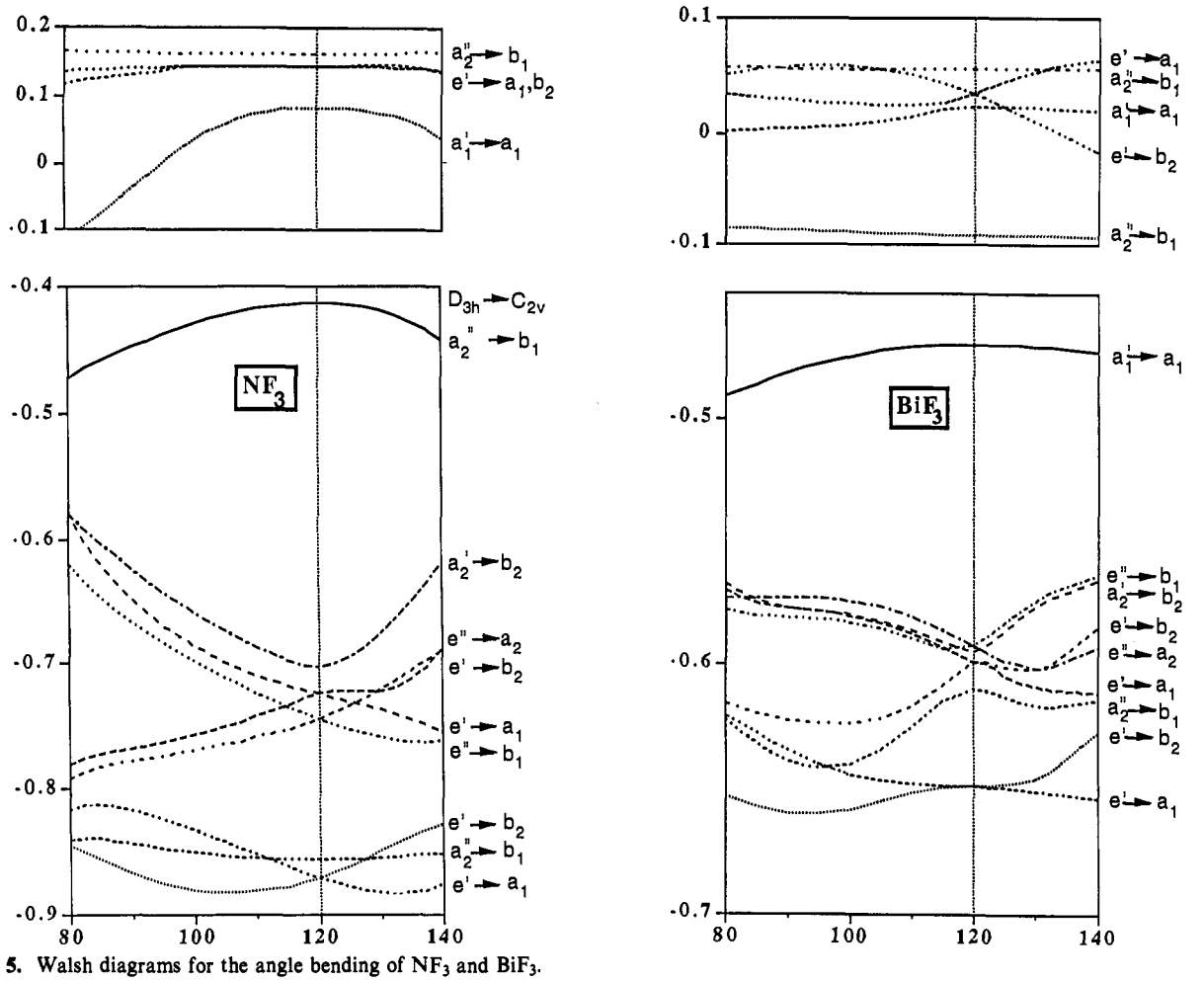

Figure 5. Walsh diagrams for the angle bending of NF_3 and BiF_3.

very similar to the ClF_3 molecule, where the HOMO is of a_1' symmetry. ClF_3 is well-known to undergo a second-order JT distortion involving an $a_1'_{HOMO} \otimes e'_{LUMO}$ mixing.[23] Hence, the change in the inversion structure from D_{3h} to C_{2v} can be rationalized by a second-order Jahn–Teller symmetry breaking. To highlight this even more we list the differences in orbital energies $\Delta\epsilon$ between the a_1' HOMO and the e' LUMO in Table 7. It is clearly seen that small $\Delta\epsilon$ values are obtained for PF_3, AsF_3, SbF_3, and BiF_3 in contrast to NF_3. We also point out that the C_{2v} minimum structures of the group 15 hydrides in the $^1A_1$ excited electronic state can also be rationalized through a second-order JT symmetry breaking.[7]

Walsh diagrams have been very useful in the discussion of molecular distortions.[5,12,80] The Walsh diagrams for the e' distortion of NF_3 and BiF_3 are compared in Figure 5. As expected, the a_1' HOMO becomes stabilized by distortion into C_{2v} symmetry toward the T-shaped structure. One also observes the usual splitting of the e orbitals by distortion in either direction. Perhaps the most significant difference between the two Walsh diagrams is that in the case of BiF_3 the most bonding orbitals exhibit minima in the region near the calculated angle of the T-shaped structure. As mentioned before,[27] the axial bond distance r^a is shorter than the equatorial bond distance r^e for all group 15 fluorides at angles $\alpha < 120°$ (and vice versa for $\alpha > 120°$, Y-shaped structure). Clotet *et al.* suggested that the a_1 HOMO becomes bonding in the axial direction but antibonding in the equatorial direction by distortion from D_{3h} to C_{2v}.[27] We do not find any bonding character toward the axial ligand since the a_1 HOMO has purely antibonding character. One may, however, argue that the a_1 HOMO becomes less antibonding in the axial direction due to the distortion into the planar T-shaped arrangement, thus strengthening the M–F^a bond. Moreover, analyzing the nature of the low-lying bonding a_1 orbital we find that it stabilizes the M–F^a bond by additional metal-p_z admixture in contrast to the M–F^e bond.

The Mulliken central-atom s population shows a remarkable difference between NF_3 and the other group 15 fluorides, Table 6. For NF_3 the Mulliken N(2s) population is *decreased* for the D_{3h} transition structure compared to the minimum arrangement. This is expected since the a_1 HOMO can be characterized as an sp hybrid transforming into a pure p orbital of a_2'' symmetry at the D_{3h} inversion point. In contrast, the other group 15 fluorides yield an increased s population at the C_{2v} transition state compared to the minimum structure. In this case, the $a_1(C_{3v})$ orbital changes into an $a_1(C_{2v})$ orbital with strong s character. It is generally believed that the central atom becomes more electronegative in the inversion toward the planar transition structure. This should be reflected in a decreased Mulliken atomic charge for the central atom M. This is the case for NF_3, SbF_3, and BiF_3 (Table 6) and for all group 15 hydrides,[7] but *not* for PF_3 and AsF_3. Hence, this assumption does not hold in general for MX_3 inversion processes.

Figure 6A shows the nonrelativistic (NR) and relativistic (R) HF angle bending potential curves of planar BiF_3 in comparison to BiH_3. It is evident that the energy gain due to distortion is larger in the NR compared to the R case. A comparison of the a_1'/e' orbital energy differences shows that $\Delta\epsilon$ is smaller at the NR compared to the R level. Hence, the second-order JT effect is expected to be larger for the NR molecule, and this rationalizes the smaller NR F–Bi–F bond angle α. In the relativistic case the D_{3h} structure is only 17 kJ/mol above the C_{2v} inversion point at the relativistic HF level, and the F–Bi–F angle is almost 90° at the relativistic MP2 level, the largest angle among all MF_3 compounds which undergo distortion. It is therefore of no surprise that a semiempirical method such as PM3 predicts a trigonal

(80) Rauk, A.; Allen, L. C.; Clementi, E. *J. Chem. Phys.* **1970**, *52*, 4133.

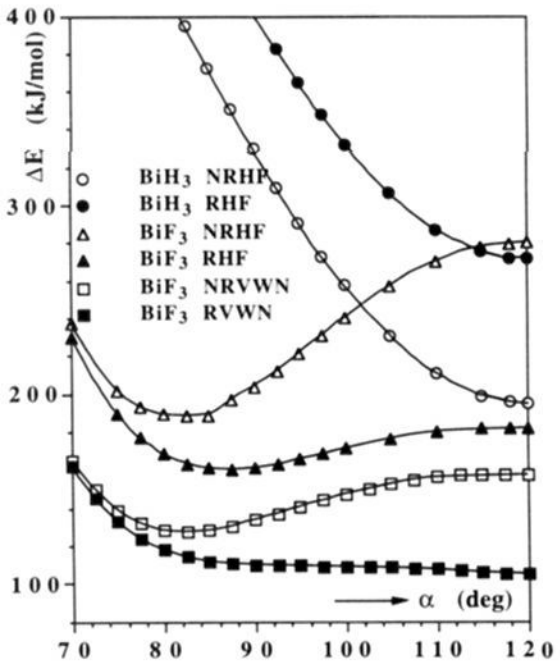

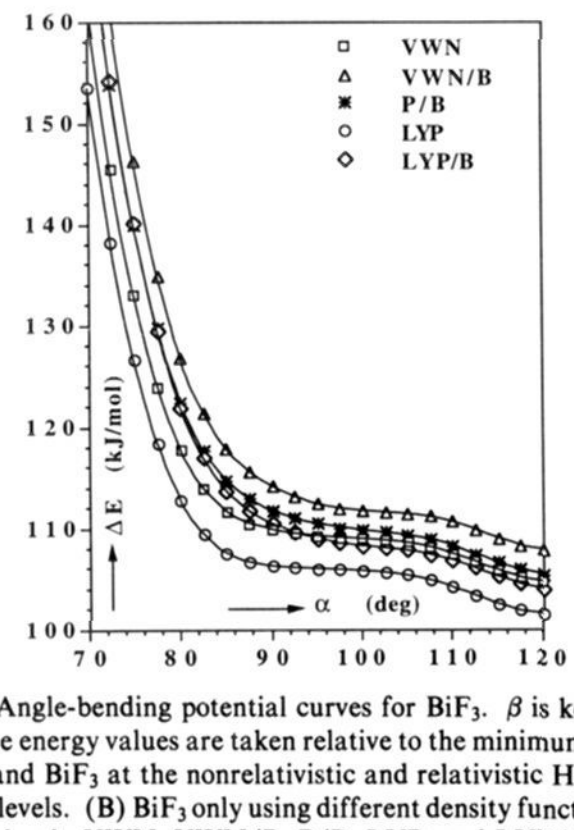

Figure 6. Angle-bending potential curves for BiF_3. β is kept constant at 90°. The energy values are taken relative to the minimum structures. (A) BiH_3 and BiF_3 at the nonrelativistic and relativistic Hartree–Fock and VWN levels. (B) BiF_3 only using different density functionals at the relativistic level: VWN, VWN/B, P/B, LYP, and LYP/B.

planar inversion structure. However, Figure 6B shows that all density functionals used with or without gradient corrections predict a trigonal planar structure for BiF_3 at the relativistic level in contrast to HF or MP2. The density functional angle bending potential curves are, however, unusual, showing a turning point at angles lower than 120° indicating the presence of some JT distortion. Note that electron correlation (MP2 versus HF) leads to large changes in the F–Bi–F angle (2.7°) compared to the other group 15 fluorides (1.4° for PF_3, 1.9° for AsF_3, and 1.9° for SbF_3). A multiconfiguration treatment of BiF_3 may lead to significant changes in the molecular geometry, but it is questionable if it would lead to a trigonal planar transition state. For example, single-reference QCISD(T)[50] geometry optimization of BiF_3 yields $r^e = 2.140$ Å, $r^a = 2.035$ Å, and $\alpha = 90.2°$ for the transition state and $r_e = 2.051$ Å and $\beta = 120.7°$ for the minimum structure; both are close to the RMP2 results (Table 1) despite the fact that the barrier of 124.5 kJ/mol is somewhat lower than the RMP2 result. The QCISD(T) method produces results of high accuracy unless there are major multireference effects, and here we find values close to the RMP2 results, suggesting that such effects are not dominant for BiF_3. Hence, the inversion structure of BiF_3 seems to be an ideal test case for the reliability of the method used. The relativistic inversion barrier of BiF_3 is lower than that of BiH_3. This is *not* entirely a consequence of the second-order JT distortion, Figure 6A. The nonrelativistic inversion barriers of BiF_3 and BiH_3 are of comparable size. However, the relativistic change in the BiF_3 inversion barrier

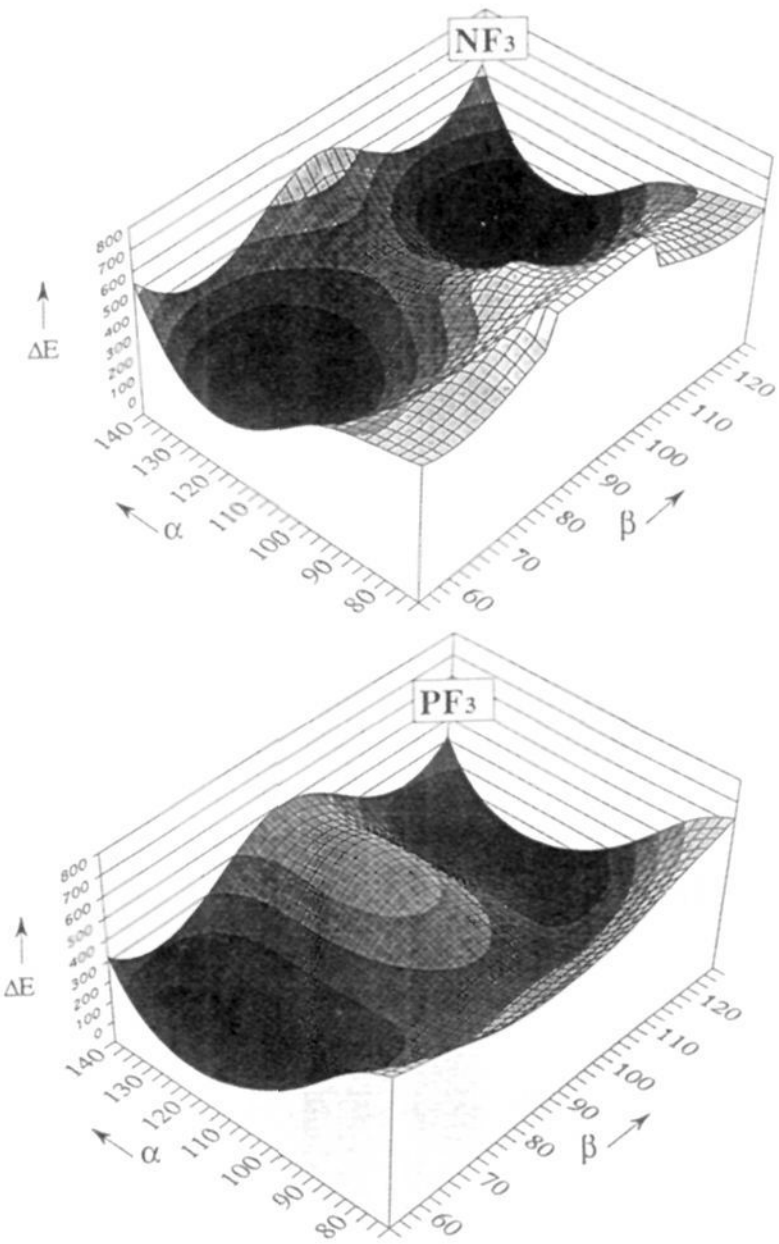

Figure 7. Hartree–Fock (α,β)-inversion hypersurfaces for NF_3 and PF_3. *The angle α denotes the F–M–C_3–F torsion angle (C_3 is the C_3-axis in* the C_{3v} point group; for the usual C_{3v} inversion, α is constant, 120°), and β is the C_3–M–X inversion angle (β is 90° at the transition state).

(Table 1) is of similar magnitude compared to BiH_3 at the trigonal planar arrangement ($\alpha = 120°$), but *opposite* in sign (Figure 6A).

At the HF level we have the D_{3h} point of the inversion hypersurface lying above the C_{3v} minimum with the following energy differences ΔE (in kJ/mol; C_{2v}/D_{3h} energy differences are set in parentheses): 499.9 (220.4) for PF_3, 375.7 (145.5) for AsF_3, 303.8 (119.8) for SbF_3, and 165.2 (16.6) for BiF_3. The D_{3h}/C_{3v} energy differences between BiH_3 and BiF_3 at the relativistic level show that $\Delta E(BiH_3,D_{3h}) > \Delta E(BiF_3,D_{3h})$. However, as mentioned before, in the high-energy region a single-reference HF or MP2 treatment may not be adequate and a MCSCF procedure can change such energy differences significantly as is the case for PF_3 (see the discussion below). For the heavier group 15 fluorides we obtain the same decreasing trend for $\Delta E(D_{3h})$ as we saw for the E_a values shown in Table 1, *i.e.*, $PF_3 > AsF_3 > SbF_3 > BiF_3$. The only exception is NF_3, where it was found that $\Delta E(NF_3,D_{3h}) < \Delta E(PF_3,D_{3h})$ as Marynick also noted in an earlier paper.[14] We attribute the large second-order JT stabilization in PF_3 as responsible for the decrease in the inversion barriers from NF_3 to PF_3.

Inversion Hypersurfaces. The inversion hypersurfaces $E(\alpha,\beta)$ for NF_3 and PF_3 are shown in Figure 7, and the contour plots of all group 15 fluorides are presented in Figure 8. The NF_3 and PF_3 hypersurfaces show nicely the two different inversion mechanisms. The D_{3h} point in PF_3 is a second-order saddle point in $E(\alpha,\beta)$ and a *third-order* saddle point in the complete PF_3 hypersurface. This is supported by analyzing the Cartesian force field at the MP2-optimized D_{3h} point which is zero in all directions. Figure 8 shows that at the D_{3h} point the molecules PF_3, AsF_3, SbF_3, and BiF_3 will undergo a second-order JT symmetry breaking

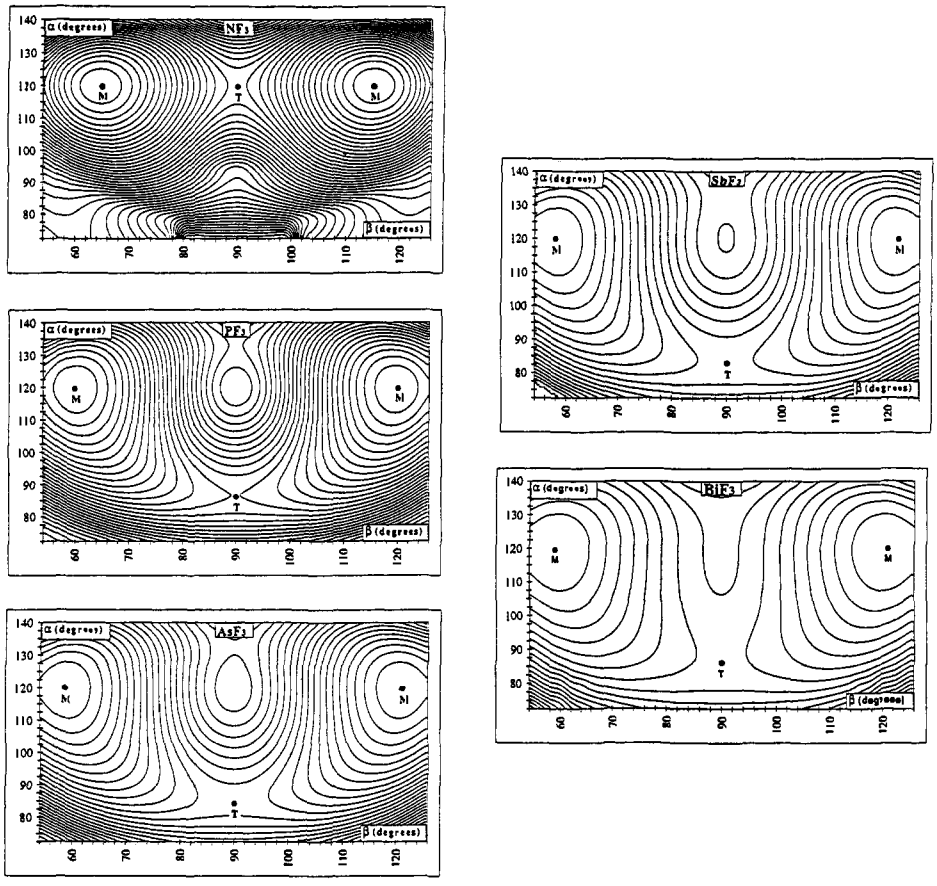

Figure 8. Hartree–Fock contour plots for the (α,β)-inversion hypersurfaces of the group 15 fluorides NF_3, PF_3, AsF_3, SbF_3, and BiF_3. The angle α denotes the F–M–C_3–F torsion angle (C_3 is the C_3-axis within the C_{3v} point group; for the usual C_{3v} inversion, α is constant, 120°), and β is the C_3–M–X inversion angle (β is 90° at the transition state). Each line represents an increase of 20 kJ/mol (minimum is set at 0 kJ/mol). The minimum and transition state are denoted as M and T, respectively. $\alpha < 120°$ leads to a T-shaped and $\alpha > 120°$ to a Y-shaped MF_3 structure.

in either direction; *i.e.*, these molecules distort into either a T-shaped or a Y-shaped structure, both of C_{2v} symmetry. The contour plots clearly show that these molecules distort immediately from the ground state C_{3v} structure into C_s symmetry when undergoing inversion, indicating that the minimum C_{3v} structure is identical with the bifurcation point. Hence, for PF_3, AsF_3, SbF_3, and BiF_3 the MEIP is of C_s symmetry starting from the minimum C_{3v} structure to the C_{2v} T-shaped transition point. The second MEIP is a high-energy path of the same symmetry (C_s) leading to a Y-shaped transition structure. At the HF level the Y-shaped saddle point is characterized by an MF_2 unit which weakly interacts with a fluorine atom and therefore may lead to the F-abstraction path of MF_3. The HF dissociation energies of $MF_3 \rightarrow MF_2 + F$ (Table 5) support this assumption; *i.e.*, for PF_3 at the HF level the Y-shaped transition structure lies 462 kJ/mol above the C_{3v} minimum. The HF dissociation limit, however, is lower than this value (332 kJ/mol). Extensive CI calculations would be necessary to obtain an accurate picture of the decomposition mechanism of MF_3 compounds.

The two different configurations (a_1' occupied versus a_2'' occupied) at the inversion point (D_{3h} and C_{2v}) do *not* belong to the same hypersurface as was suggested by Arduengo and Dixon[11] as well as Clotet *et al.*;[27] *i.e.*, NF_3 shows *no* additional saddle point at an angle α lower than 120° and PF_3 has *no* additional second-order saddle point at the D_{3h} structure for the ground state potential energy surface. Both configurations (a_1' occupied versus a_2'' occupied) can, of course, be directly incorporated in the calculations through a CI procedure. Hence, both the above configurations belong to two different hypersurfaces of the same symmetry (ground and excited state), with one particular inversion pathway expected to be the dominant one for the ground-state hypersurface, *i.e.*, the C_{3v} MEIP for NF_3 and the C_s MEIP for PF_3, AsF_3, SbF_3, and BiF_3. Therefore, the C_{2v} structures for the group 15 hydrides and the D_{3h} structures for PF_3, AsF_3, and SbF_3 reported by Dixon and Arduengo[11] belong to an electronically excited state hypersurface.

The contour plots in Figures 7 and 8 show that the barrier heights of the early fluorides (NF_3 and PF_3) are very high and could be above the dissociation limit of either of the decomposition reactions $MF + F_2$ or $MF_2 + F$. Since ground-state F_2 is of singlet symmetry and the first excited state of F_2 ($^3\Pi$) is ca. 25 500 cm^{-1} above the $^1\Sigma_g^+$ ground state,[74] one of the dissociation limits of the potential energy surface is characterized by MF_3 ($^1A_1$; C_{3v}) → MF ($^1\Delta$) + F_2 ($^1\Sigma_g^+$). However, the ground-state symmetry of all group 15 MF compounds is of $^3\Sigma^-$ symmetry and, therefore, there exists a crossing between singlet and triplet hypersurfaces toward the dissociation limit. This suggests that the study of the MF_3 decomposition can become quite complicated. We also checked possible crossings at the high-energy D_{3h} inversion point of NF_3. However, at the D_{3h} point the next excited $^3A_2''$ state is 150 kJ/mol above the $^1A_1'$ state at the HF level. Figure 2 shows a comparison between the MP2 inversion barriers and the energetics of the two energetically accessible decomposition reactions of MF_3 compounds (see also Table 5). Only for NF_3 the inversion barrier is above the dissociation limit (at the MP2 level). However, more accurate CI calculations are necessary since MP2 results for $NF(^3\Sigma^-)$ may not be adequate. For the heavier fluorides our results indicate that the inversion barrier will be below the decomposition limit (even at a CI level).

For the group 15 fluorides both configurations (a_1' occupied, a_2'' occupied) are important and Freed's theorem,[81] which states and electron correlation does not play a major role in the inversion process, is not valid.[11] Indeed, a comparison between the HF and MP2 values shows rather large differences in the barrier heights

(81) Freed, K. F. *Chem. Phys. Lett.* **1968**, *2*, 566.

(however, MP2 may overestimate correlation effects; see ref 53). Electron correlation increases the F–M–F (M = P, As, Sb, and Bi) angle α at the transition state and decreases E_a (in contrast to NF_3 at the P2 level), therefore stabilizing more the trigonal planar form. This can be understood since the major configuration mixing into the ground state is one with the a_2'' as HOMO, *i.e.*, the one preferring the D_{3h} inversion structure. However, since the structure at the inversion point is changing significantly with electron correlation, we again point out that an MCSCF procedure would be more appropriate, as has been mentioned before by Boggs and Seida.[82] Around the minimum a single-reference treatment is sufficient. Distortion occurs immediately upon changing the inversion angle β, as can be seen in the contour plots for all group 15 fluorides (Figure 6). This indicates that the symmetry breaking from C_{3v} into C_s would also require a multiconfiguration treatment. To analyze the importance of electron correlation for such hypersurfaces in more detail, we carried out CASPT2 calculations for the ground-state minimum and inversion structure of NF_3 and PF_3.

Multireference MP2 Calculations for NF_3 and PF_3. The Walsh diagram of BiF_3 (which is similar to that of PF_3) in Figure 5 shows that the most important configurations are obtained by occupying the a_1' HOMO and the first seven LUMOs which are of a_2'', e', and a_1' symmetry (similarly for the C_{2v} and C_{3v} structures). These define the eight active orbitals giving 40 CSFs used in the CASSCF procedure for NF_3 and PF_3. Table 1 shows that for the C_{2v} structure of PF_3 the CASPT2 results are quite different from the results of the single-reference MP2 approach. The JT symmetry breaking for PF_3 is also obtained at the CASPT2 level, and we are therefore confident that the distortion is a true physical effect, supporting Dixon and Arduengo's earlier conclusion.[11] The minimum bond distances become slightly smaller and agree now much better with the experimental results. As expected, the distortion angle α at the T-shaped transition state increases by 1.0° for PF_3 because of the large admixture of the b_1 component (a_2'' in D_{3h}). This becomes evident when listing the CASSCF occupation numbers for the two frontier orbitals of the transition state of PF_3 (C_{2v} symmetry), 1.883 for the a_1 orbital and 0.093 for the b_1 orbital. This is in contrast to NF_3 in the D_{3h} transition state with the a_2'' orbital (b_1 in C_{2v}) being now occupied, *i.e.*, 0.0005 for the frontier a_1' orbital (a_1 in C_{2v}) and 1.941 for the a_2'' orbital. The D_{3h} structure of PF_3 is 103.9 kJ/mol above the C_{2v} structure at the CASPT2 level, which is now considerably lower than the HF result (220.4 kJ/mol) and the single-determinant MP2 value (124.0 kJ/mol). Again, this is expected because of the b_1 admixture favoring D_{3h} symmetry, Figure 4. Note that this results in $\Delta E(NF_3;D_{3h}) \approx \Delta E(PF_3;D_{3h})$ in contrast to the HF or MP2 results. It is interesting to compare the coefficients for the dominant CASSCF CSF at different points of the PF_3 (NF_3) hypersurface: 0.985 (0.992) for the C_{3v} minimum structure, 0.970 for the C_{2v} transition state, and 0.892 (0.985) for the D_{3h} point. Hence, the largest deviation from a single-reference treatment occurs at the D_{3h} point for PF_3. Therefore, the bond distances at the trigonal planar arrangement can change significantly between the different methods (for PF_3: HF, 1.679 Å; MP2, 1.705 Å; and CASPT2, 1.653 Å). The barrier height is reduced for NF_3 (–37.6 kJ/mol) and PF_3 (–29.9 kJ/mol) when changing from MP2 to the CASPT2 level. Hence, even for NF_3, which does not show significant admixtures by excited CSFs at the D_{3h} point, we nevertheless obtain relatively large correlation contributions to the inversion barrier. We expect similar changes for the heavier group 15 fluorides. Finally we note that the total electronic energy E of the CASPT2 calculation is above the single-reference MP2 value, indicating that the single-reference MP2 procedure overestimates electron correlation. For example, at the CASPT2 minimum structure of NF_3 (PF_3) we obtain E = –353.515 94 au (–640.021 56 au) compared to the single-reference MP2 result of E = –353.543 39 au (–640.031 06 au).

(82) Boggs, J. E.; Seida, D. *J. Chem. Phys.* **1981**, *75*, 3645.

IV. Conclusion

We draw the following conclusions:

(a) C_{3v} symmetry breaking in the inversion process can be explained by a second-order JT distortion. We point out, however, that we have used frontier orbital theory, a method which has been criticized as inaccurate by Ballhausen.[83] This is evident as the differences in orbital energies cannot explain completely the decreasing trend in the group 15 fluoride activation barriers. Moreover, it may not be appropriate to use energies of virtual canonical orbitals because they are very basis set dependent and have little physical meaning. There may be, of course, other models available to rationalize such a behavior. However, Figure 4 shows that the widely used VSEPR model is unable to explain the unusual transition-state structures of the heavier group 15 fluorides.

(b) The change in the HOMO symmetry from a_2'' into a_1' as we move down the period may be rationalized using electronegativity arguments.

(c) A detailed study of HF hypersurfaces for the MF_3 inversion process shows that PF_3, AsF_3, SbF_3, and BiF_3 distort immediately if the angle β is decreased toward the planar transition structure. This results in a C_s MEIP. NF_3 follows the usual C_{3v} MEIP.

(d) CASPT2 calculations for NF_3 and PF_3 confirm the MP2 results, and therefore, the original analysis given by Dixon and Arduengo[11] is valid. However, more accurate information on the inversion structure and barrier is obtained from this multireference electron correlation procedure.

(e) Density functional approximation and MP2 predict different inversion structures for BiF_3 at the relativistic level. This is mainly due to the very shallow distortion curve from the trigonal to the T-shaped planar arrangement. In the nonrelativistic case both methods predict the transition state to be T-shaped. We conclude that high-level electron correlation procedures and larger basis sets are necessary to decide upon the correct inversion structure. However, relativistic calculations on the inversion state of BiF_3 using a coupled-cluster procedure support our MP2 result of a T-shaped structure. More advanced density functional techniques together with extended basis sets will be required to determine if the LDA with gradient corrections is able to give results similar to those obtained from *ab-initio* calculations. Thus this is a nice example of a second-order JT effect which may lead to a distortion (MP2) or not (VWN, LYP, ...).

(f) The LDA performs reasonably well when compared to MP2 for the compounds presented in this work. However, adding the nonlocal Becke correction leads to bond distances that are too large and to frequencies with large deviations from the experimental results.

(g) Large relativistic effects are calculated for the F–Bi–F minimum angle in BiF_3, resulting in an anomalous trend in the group 15 F–M–F bond angles from M = F to M = Bi.

(h) Vibrational data are predicted for the ν_4(E) mode of SbF_3 and the vibrational spectrum of BiF_3.

(i) There remains an interesting problem to be solved: *Why is the minimum structure of the fluorides which undergo distortion of exact C_{3v} symmetry*? The second-order JT term must be zero at the minimum geometry (neglecting higher order terms), and hence, the minimum is identical with the bifurcation point.

We feel that in order to develop accurate hypersurfaces for these systems a multireference treatment of electron correlation is required for the group 15 hydrides and fluorides. Especially in high-energy regions of the hypersurfaces, the wave function will have strong multiconfiguration character. It would be

(83) (a) Ballhausen, C. J. *J. Chem. Phys.* **1970**, *53*, 2986. (b) Pearson, R. *J. Chem. Phys.* **1970**, *53*, 2986.

interesting in this context to determine if the first two excited states of the same symmetry as the ground state undergo a JT distortion as well. It would also be useful to analyze the JT terms in detail and verify our rationalization of these inversion processes.

Finally we note that it would be very difficult to verify these unusual inversion structures experimentally. However, since the distortion is evident around the minimum, large anharmonicity effects are expected in the bending potential, and therefore, third and fourth energy derivatives with respect to the F–Bi–F bending angle should not be small, and this could indicate a distortion from the usual C_{3v} MEIP. In addition, for inversion processes through the usual trigonal planar geometry the dipole moment of the molecule is zero at the inversion point, $\mu = 0$. This is, of course, *not* the case if a second-order JT distortion takes place into the T-shaped structure, i.e., $\mu \neq 0$. Hence, one may expect anomalies in the dipole moment $\mu(n)$ with increasing vibronic quantum number n for the $\nu_2(A_1)$ inversion mode. It would therefore be interesting to study the microwave spectra of group 15 fluorides in more detail using high-resolution spectroscopy.

Acknowledgment. We are grateful for financial support by the Auckland University Research Committee, the New Zealand Vice Chancellors Committee, the New Zealand Lottery Science Research Committee, and the Alexander von Humboldt Stiftung. We thank Dr. Josef Ischtwan for helpful comments.